

1 **Heterogeneous chemistry: a mechanism missing in**  
2 **current models to explain secondary inorganic**  
3 **aerosol formation during the January 2013 haze**  
4 **episode in North China**

5 **B. Zheng<sup>1</sup>, Q. Zhang<sup>2,5</sup>, Y. Zhang<sup>3,1,5</sup>, K. B. He<sup>1,4,5</sup>, K. Wang<sup>3</sup>, G. J. Zheng<sup>1</sup>,**  
6 **F. K. Duan<sup>1</sup>, Y. L. Ma<sup>1</sup>, and T. Kimoto<sup>6</sup>**

7  
8 [1] {State Key Joint Laboratory of Environment Simulation and Pollution Control,  
9 School of Environment, Tsinghua University, Beijing, China}

10 [2] {Ministry of Education Key Laboratory for Earth System Modeling, Center for  
11 Earth System Science, Tsinghua University, Beijing, China}

12 [3] {Department of Marine, Earth and Atmospheric Sciences, North Carolina State  
13 University, Raleigh, North Carolina, USA}

14 [4] {State Environmental Protection Key Laboratory of Sources and Control of Air  
15 Pollution Complex, Beijing 100084, China}

16 [5] {Collaborative Innovation Center for Regional Environmental Quality, Beijing  
17 100084, China}

18 [6] {Kimoto Electric Co., Ltd, 3-1 Funahashi-cho Tennoji-ku Osaka, 543-0024 Japan}

19

20

21

22

23

24

25

26

27

28 Correspondence to: Q. Zhang ([qiangzhang@tsinghua.edu.cn](mailto:qiangzhang@tsinghua.edu.cn))

29 K. B. He ([hekb@tsinghua.edu.cn](mailto:hekb@tsinghua.edu.cn))

## Abstract

Severe regional haze pollution events occurred in eastern and central China in January 2013, which had adverse effects on the environment and public health. Extremely high levels of particulate matter with aerodynamic diameter of 2.5  $\mu\text{m}$  or less ( $\text{PM}_{2.5}$ ) with dominant components of sulfate and nitrate are responsible for the haze pollution. Although heterogeneous chemistry is thought to play an important role in the production of sulfate and nitrate during haze episodes, few studies have comprehensively evaluated the effect of heterogeneous chemistry on haze formation in China by using the 3D models due to of a lack of treatments for heterogeneous reactions in most climate and chemical transport models. In this work, the WRF-CMAQ model with newly added heterogeneous reactions is applied to East Asia to evaluate the impacts of heterogeneous chemistry and the meteorological anomaly during January 2013 on regional haze formation. **As the parameterization of heterogeneous reactions on different types of particles are not well established yet, we first took the update coefficients from reactions on dust particles and then conducted several sensitivity runs to find the value that can best match observations.** The revised CMAQ with heterogeneous chemistry not only captures the magnitude and temporal variation of sulfate and nitrate, but also reproduces the enhancement of relative contribution of sulfate and nitrate to  $\text{PM}_{2.5}$  mass from clean days to polluted haze days. These results indicate the significant role of heterogeneous chemistry in regional haze formation and improve the understanding of the haze formation mechanisms during the January 2013 episode.

## 54 1. Introduction

55 Regional haze pollution is an atmospheric phenomenon characterized by  
56 significant growth in the concentration of aerosol particles and sharp reduction of  
57 visibility. In addition to the adverse effects on visibility, haze pollution also affects the  
58 air quality, public health, and climate. By scattering and absorbing solar radiation,  
59 aerosol particles suspended within haze can decrease the fluxes of solar radiation  
60 reaching the earth's surface, significantly altering the earth's energy budget and  
61 climate (Seinfeld et al., 2004; Mercado et al., 2009). Sulfate and nitrate aerosols can  
62 increase soil acidity through acid deposition, which has a negative impact on the  
63 ecosystem (Zhao et al., 2009). Because of their small sizes, aerosol particles can  
64 penetrate deeply into human lungs, causing respiratory diseases, decreased lung  
65 function, and increased risk of cancer and mortality (American Lung Association,  
66 2006).

67 Haze pollution in China is of significant concern because of its increased  
68 frequency of occurrence in recent years. The number of haze days has shown an  
69 increasing trend since the 1990s and visibility during the haze events has decreased  
70 rapidly (Zhao et al., 2011; Ding and Liu, 2014). Aerosol loadings during haze days  
71 can be extremely high with maximum hourly concentrations of particulate matter with  
72 aerodynamic diameter of 2.5  $\mu\text{m}$  or less ( $\text{PM}_{2.5}$ ) of 200–1000  $\mu\text{g m}^{-3}$  (Sun et al., 2006;  
73 Wang et al., 2006; X. J. Zhao et al., 2013; L. T. Wang et al., 2014; Y. S. Wang et al.,  
74 2014), which can reduce surface solar radiation by more than 20  $\text{W m}^{-2}$  (Li et al.,  
75 2007).

76 Most parts of central and eastern China experienced a persistent episode of haze  
77 pollution during January 2013, which is one of the most severe air pollution episodes  
78 in China during the last decade (He et al., 2014; Y. S. Wang et al., 2014; Z. F. Wang et  
79 al., 2014; J. K. Zhang et al., 2014; R. H. Zhang et al., 2014). Widespread haze clouds  
80 covered the entire North China Plain (NCP) (Yang et al., 2013) and the instantaneous  
81 concentration of  $\text{PM}_{2.5}$  within these clouds exceeded 1000  $\mu\text{g m}^{-3}$  at some urban  
82 observational sites (Y. S. Wang et al., 2014). The characteristics and formation  
83 mechanisms of this haze event attract considerable attention from the scientific  
84 community.

85 High emission intensity, adverse meteorological conditions, and the formation of  
86 substantial amounts of secondary aerosols are generally regarded as the principal  
87 factors underlying the formation of the severe haze pollution in January 2013. Central

88 and eastern China are the most important source regions of anthropogenic emissions  
89 in China (Zhang et al., 2009), which can provide sufficient precursors for haze  
90 formation. Adverse meteorological conditions in January 2013 conducive to haze  
91 formation include weak surface winds, low mixing layers, a thick temperature  
92 inversion layer, and anomalous southerly winds in the middle and lower troposphere  
93 that transport large amounts of water vapor and pollutants (Y. S. Wang et al., 2014; R.  
94 H. Zhang et al., 2014). Under weather conditions of high humidity and reduced  
95 advection and vertical mixing, large amounts of secondary aerosols (both organic and  
96 inorganic) can be generated. In particular, greater amounts of secondary inorganic  
97 aerosols comprising sulfate, nitrate, and ammonium (SNA) were produced during the  
98 haze days of the January 2013 episode than during clean days. The contribution of  
99 sulfate and nitrate to PM<sub>2.5</sub> increased from 10.3–13.4% and 6.6–14% in clean days to  
100 25.1% and 17.5–20.6% in haze days, respectively (J. K. Zhang et al., 2014; Quan et  
101 al., 2014). The total contribution of SNA reached about 60% during the most severe  
102 haze days from 12–15 January (J. K. Zhang et al., 2014; Quan et al., 2014), which  
103 indicates that the significant production of SNA is a principal driving force that leads  
104 to the sharp increase in PM<sub>2.5</sub> concentrations.

105 Many studies on aerosols have revealed that SNA are the most abundant  
106 component of PM<sub>2.5</sub> during haze pollution events in China, and that the processes and  
107 evolution of haze pollution are characterized by the formation of substantial amounts  
108 of sulfate and nitrate (Sun et al., 2006; Wang et al., 2006; X. J. Zhao et al., 2013). The  
109 formation mechanisms are difficult to be explained by traditional gas-phase or  
110 aqueous-phase chemistry (i.e., gas-phase oxidation by hydroxyl radical (OH) and in-  
111 cloud oxidation by dissolved ozone (O<sub>3</sub>) and hydrogen peroxide (H<sub>2</sub>O<sub>2</sub>)) given the  
112 adverse atmospheric conditions (i.e. low or even zero O<sub>3</sub> concentrations, dim days  
113 with low solar radiations and few precipitating clouds) (X.J. Zhao et al., 2013; Quan  
114 et al., 2014). Besides the gas-phase and aqueous-phase chemistry, heterogeneous  
115 chemistry is considered to be alternative pathways of sulfate and nitrate formation in  
116 the atmosphere (Ravishankara, 1997). The ambient measurement has verified the  
117 existence of heterogeneous reactions associated with sulfur dioxide (SO<sub>2</sub>), nitrogen  
118 pentoxide (N<sub>2</sub>O<sub>5</sub>) and nitric acid (HNO<sub>3</sub>) (Usher et al., 2003; Lammel and Leip, 2005;  
119 McNaughton et al., 2009; Chang et al., 2011). Field studies during haze days in China  
120 proposed that the large amount of sulfate and nitrate were more likely generated via  
121 heterogeneous chemistry than gas-phase and aqueous-phase chemistry (Wang et al.,

122 2006; Li and Shao, 2009, 2010; Li et al., 2011; X. Wang et al., 2012; X. J. Zhao et al.,  
123 2013; Y. S. Wang et al., 2014). Modeling studies have used 0-3D air quality models to  
124 research on the role of heterogeneous reactions in sulfate and nitrate formation on the  
125 surface of mineral particles (Zhang et al., 1994; Dentener et al., 1996; Zhang and  
126 Carmichael, 1999; K. Wang et al., 2012). However, few studies have comprehensively  
127 evaluated the effect of heterogeneous chemistry on haze formation in China by using  
128 the 3D models because of a lack of treatments for heterogeneous reactions in most  
129 climate and chemical transport models.

130 In this work, we use the CMAQ model to investigate the impact of  
131 heterogeneous chemistry on the severe regional haze formation in January 2013. The  
132 officially-released version of CMAQ (hereafter the original CMAQ) and revised  
133 CMAQ with updated treatments for heterogeneous chemistry by adding a number of  
134 reactions (hereafter the revised CMAQ) are applied to simulate the January 2013  
135 severe regional haze pollution episode over East Asia. Our objectives are to improve  
136 the model's capability in reproducing the observed high PM concentrations and  
137 provide better understanding of the effects of heterogeneous reactions on the  
138 production of sulfate and nitrate during the haze event.

139

## 140 **2. Model Description and Methodology**

141 In this work, the Weather Research and Forecasting (WRF) model v3.5.1  
142 (<http://www.wrf-model.org/>) and CMAQ v5.0.1 (<http://www.cmascenter.org/cmaq/>)  
143 are applied to simulate the severe haze episode in January 2013 over East Asia. WRF  
144 is a new generation mesoscale numerical weather prediction system designed to serve  
145 a wide range of meteorological applications from meters to thousands of kilometers  
146 (<http://www.wrf-model.org/>). WRF v3.5.1 is the most recent major WRF release in  
147 September 2013 and is used to generate meteorological fields to drive CMAQ.  
148 CMAQ is a 3D Eulerian atmospheric chemistry and transport modeling system that  
149 simulates multi pollutants throughout the troposphere across spatial scales ranging  
150 from local to hemispheric. CMAQ v5.0.1 is the most up to date release in July 2012.  
151 It contains the updated carbon bond gas-phase mechanism with new toluene  
152 chemistry (Whitten et al., 2010), a new aerosol module (AERO6), and ISORROPIA  
153 v2.1 inorganic chemistry (Fountoukis and Nenes, 2007). The existing formation  
154 mechanisms for SNA included in the original CMAQ and new heterogeneous  
155 reactions added in the revised CMAQ that form additional SNA are described below.

## 156 2.1. The Formation Mechanisms of SNA in the Original CMAQ

157 Table 1 summarizes major mechanisms for sulfate and nitrate formation  
158 currently treated in the original CMAQ v5.0.1 (R1–R15) in a highly simplified  
159 manner. In the gas-phase (R1–R6), sulfuric acid ( $\text{H}_2\text{SO}_4$ ) and  $\text{HNO}_3$  are generated  
160 mainly through the oxidation of  $\text{SO}_2$  and nitrogen oxide ( $\text{NO}_x$ ) by OH. Additional  
161  $\text{HNO}_3$  can be formed through subsequent reactions involving reactive nitrogen species  
162 such as nitrogen trioxide ( $\text{NO}_3$ ),  $\text{N}_2\text{O}_5$ , and NTR and OH, hydroperoxyl radical ( $\text{HO}_2$ ),  
163 and  $\text{H}_2\text{O}$  as well as the nighttime oxidation reaction of volatile organic compounds  
164 (VOCs) by  $\text{NO}_3$ .  $\text{H}_2\text{SO}_4$  and  $\text{HNO}_3$  can condense on the surface of preexisting  
165 aerosol, forming sulfate ( $\text{SO}_4^{2-}$ ) and nitrate ( $\text{NO}_3^-$ ). For in-cloud chemistry (R7–R13),  
166 the original CMAQ includes the dissolution equilibria of  $\text{SO}_2$ ,  $\text{H}_2\text{SO}_4$ , ammonia  
167 ( $\text{NH}_3$ ),  $\text{NO}_x$ ,  $\text{NO}_3$ ,  $\text{N}_2\text{O}_5$ , nitrous acid ( $\text{HNO}_2$ ),  $\text{HNO}_3$ , peroxyntiric acid ( $\text{HNO}_4$ ), and  
168 several oxidants such as OH,  $\text{H}_2\text{O}_2$ , and  $\text{O}_3$ , the dissociation equilibria of  $\text{SO}_2$ ,  
169 bisulfite ( $\text{HSO}_3^-$ ),  $\text{HNO}_2$ ,  $\text{HNO}_3$ , and  $\text{NH}_3 \cdot \text{H}_2\text{O}$ , and five aqueous-phase kinetic  
170 reactions to produce S (VI) through the oxidation of S (IV) (dissolved  $\text{SO}_2$ ,  $\text{HSO}_3^-$   
171 and sulfite ( $\text{SO}_3^{2-}$ )) by  $\text{H}_2\text{O}_2$ , methylhydroperoxide (MHP), peroxyacetic acid (PAA),  
172  $\text{O}_3$ , and oxygen ( $\text{O}_2$ ) catalyzed by ferric iron ( $\text{Fe}^{3+}$ ) and manganese ion ( $\text{Mn}^{2+}$ ). Once  
173 clouds dissipate,  $\text{SO}_4^{2-}$  formed in the aqueous-phase becomes part of aerosol. The  
174 original CMAQ only includes two heterogeneous reactions (R14–R15) to produce  
175  $\text{HNO}_3$ , one involving  $\text{N}_2\text{O}_5$  and  $\text{H}_2\text{O}$  and the other involving nitrogen dioxide ( $\text{NO}_2$ )  
176 and  $\text{H}_2\text{O}$ . The mechanism of heterogeneous chemistry is much more complex than the  
177 homogeneous gas and aqueous-phase mechanisms. It involves many processes  
178 including water condensation onto the particle surfaces, adsorption and  
179 accommodation of gases into the liquid–gas interface, diffusion, and surface reactions  
180 (Reid and Sayer, 2003). Heterogeneous reaction rates are dependent on relative  
181 humidity (RH) (Dentener et al., 1996; Henson et al., 1996; Stutz et al., 2004) because  
182 of the significant role of the water film on the aerosol surface in the gas uptake. The  
183 formation of ammonium ( $\text{NH}_4^+$ ) is closely related to that of  $\text{SO}_4^{2-}$  and  $\text{NO}_3^-$ , as it is  
184 resulted from the neutralization of  $\text{SO}_4^{2-}$  and  $\text{NO}_3^-$  by dissolved  $\text{NH}_3$  in the  
185 particulate-phase through aerosol equilibrium treated in ISORROPIA II of Fountoukis  
186 and Nenes (2007).

## 2.2. Missing Heterogeneous Reactions and Their Implementation into Original CMAQ

Heterogeneous chemistry might have played a significant role in the January 2013 haze episode for three reasons. First, the total amount of  $\text{SO}_4^{2-}$  formed through gas- and aqueous-phase chemistry is too low to explain the observed abrupt increases in the concentrations of  $\text{SO}_4^{2-}$  by  $70\text{-}130\ \mu\text{g m}^{-3}$  within a few hours during the haze episode. The observed concentrations of  $\text{SO}_2$  are in the range of  $10\text{-}216\ \mu\text{g m}^{-3}$  (Fig. 1). The gas-phase oxidation of  $\text{SO}_2$  by OH radicals can convert  $\text{SO}_2$  to  $\text{H}_2\text{SO}_4$  at a maximum rate of  $2\% \text{ h}^{-1}$  under sunny conditions, leading to  $0.2\text{-}5.5\ \mu\text{g m}^{-3} \text{ h}^{-1}$   $\text{H}_2\text{SO}_4$  (which is equivalent to  $0.2\text{-}5.4\ \mu\text{g m}^{-3} \text{ h}^{-1}$   $\text{SO}_4^{2-}$ ). Aqueous-phase chemistry shown in Table 1 can enhance  $\text{SO}_4^{2-}$  formation in precipitating clouds, which did not occur frequently during the episode. Only two precipitations are recorded in the central China on 20-21 and 30-31 January respectively, which contribute 92% of the total precipitations in January (data derived from <http://cdc.cma.gov.cn>). Meanwhile the weak photochemical activity during dim haze days, characterized by extremely low or even zero  $\text{O}_3$  concentrations (He et al., 2014; Y. S. Wang et al., 2014), does not support that gas and aqueous-phase chemistry are dominant pathways for sulfate and nitrate production. As shown in Table 1, the original CMAQ only includes two heterogeneous reactions to produce  $\text{HNO}_3$  and does not include any heterogeneous reactions to produce  $\text{SO}_4^{2-}$ . The original model evaluation against ground-based measurements (as shown in Sect. 4.2.1) shows significant underpredictions of SNA (e.g., normalized mean biases (NMBs) of  $-40\%$  to  $-60\%$ ). These data analysis and modeling results indicate that the heterogeneous chemistry probably have played a significant role to produce high SNA during the haze pollution. Second, there exist strong correlations between RH and sulfur and nitrogen oxidation ratios (SOR and NOR) during haze in January 2013 (Sun et al., 2014; Y. S. Wang et al., 2014; G. J. Zheng et al., 2014), which resemble the RH-dependence of heterogeneous chemistry. Third, transmission electron microscopy studies have shown that the particles sampled during haze days in the NCP are mostly combined with obvious coatings containing significant sulfur and nitrogen elements, probably generated via some reactions on the particle surfaces (Li and Shao, 2009, 2010; Li et al., 2011). It suggests that surface reactions, probably caused by heterogeneous chemistry, play a significant role in haze formation. Based on the above three reasons, heterogeneous

220 chemistry is regarded as the most important missing reaction pathway and nine new  
221 heterogeneous reactions (R16–R24) are then incorporated into CMAQ to improve its  
222 capability in reproducing the high SNA concentrations observed during the haze  
223 episode through increasing sulfate and nitrate formation. Simulations from the  
224 original and the revised CMAQ are compared to study the role of heterogeneous  
225 chemistry in producing sulfate and nitrate during this haze episode, which is presented  
226 in Sect. 4.2 and 4.3.

227 As shown in Table 1, following the work of [K. Wang et al. \(2012\)](#), nine  
228 heterogeneous reactions involving H<sub>2</sub>O<sub>2</sub>, HNO<sub>3</sub>, HO<sub>2</sub>, N<sub>2</sub>O<sub>5</sub>, NO<sub>2</sub>, NO<sub>3</sub>, O<sub>3</sub>, OH, and  
229 SO<sub>2</sub> (R16–R24) have been incorporated into original CMAQ. These reactions are  
230 assumed to occur on the surface of aerosols. Heterogeneous chemistry is commonly  
231 parameterized using a pseudo-first-order rate constant and is assumed to be  
232 irreversible (Zhang and Carmichael, 1999; Jacob, 2000). The rate constant  $k$  (s<sup>-1</sup>) for  
233 heterogeneous loss of gaseous pollutants is determined by (Jacob, 2000; [K. Wang et](#)  
234 [al., 2012](#))

235

$$236 \quad k_i = \left( \frac{d_p}{2D_i} + \frac{4}{v_i \gamma_i} \right)^{-1} S_p \quad (1)$$

237

238 where  $i$  represents the reactant for heterogeneous reactions,  $d_p$  is the effective  
239 diameter of the particles (m),  $D_i$  is the gas-phase molecular diffusion coefficient for  
240 reactant  $i$  (m<sup>2</sup> s<sup>-1</sup>),  $v_i$  is the mean molecular speed of reactant  $i$  in the gas phase,  $\gamma_i$  is  
241 the uptake coefficient for reactant  $i$  (dimensionless), and  $S_p$  is the aerosol surface area  
242 per unit volume of air (m<sup>2</sup> m<sup>-3</sup>). The parameters  $d_p$ ,  $D_i$ ,  $v_i$ , and  $S_p$  are calculated in  
243 CMAQ, and the parameter  $\gamma_i$  is determined for different reactants based on laboratory  
244 measurements reported in the literatures, which is presented below.

245 The values of  $\gamma$  for different gaseous pollutants may vary several orders of  
246 magnitude, because of different surface properties, particle compositions,  
247 temperature, RH, and laboratory conditions. For a specific combination of particle and  
248 gaseous pollutants, the value of  $\gamma$  is highly dependent on RH and increases rapidly as  
249 a function of RH (Dentener et al., 1996; Henson et al., 1996; Stutz et al., 2004). For  
250 example, Mogili et al. (2006) found that the  $\gamma$  of N<sub>2</sub>O<sub>5</sub> increased by a factor of 4 as  
251 RH increased in an environmental aerosol chamber. Liu et al. (2008) reported that the  
252  $\gamma$  of HNO<sub>3</sub> on calcium carbonate was enhanced in laboratory experiments by a factor



253 of 15 over a wide range of RHs (from 20–80%). Enhanced  $\gamma$  of HNO<sub>3</sub> with increasing  
 254 RH have also been reported on many types of particles including oxides, clay, and  
 255 dust. Considering the significant effect of RH on  $\gamma$ , some modeling studies used RH-  
 256 dependent  $\gamma$  (Song and Carmichael, 2001; Wei, 2010). For example, Song and  
 257 Carmichael (2001) used a value of  $\gamma$  of 0.005 for SO<sub>2</sub> when the RH was lower than  
 258 50% and of 0.05 when RH was higher than 50%.

259 The  $\gamma$  for heterogeneous reactions used in this work are determined mainly based  
 260 on the work of K. Wang et al. (2012), which used lower and upper limits to represent  
 261 a range of  $\gamma$  values reported in the laboratory measurement. On the basis of the lower  
 262 and upper limits, we then use a piecewise function to resemble the RH-dependence of  
 263  $\gamma$ . Field measurements during the January 2013 haze episode in Beijing indicate that  
 264 the SOR and NOR are highly dependent on RH. They are relatively stable when RH is  
 265 lower than 40–50% and rapidly increase when RH is higher. The RH value of 50% is  
 266 close to the deliquescence point of particles for a mixture of organic compounds and  
 267 ammonium sulfate (Peckhaus et al., 2012), which constitute about 80% of PM<sub>2.5</sub> in  
 268 China (Yang et al., 2011). In this work, we assume the value of  $\gamma$  to be the lower limit  
 269 for  $RH \leq 50\%$  and that it increases linearly to the upper limit as RH increases to  
 270  $RH_{\max}$ , which approximates the correlation between RH and  $\gamma$ . The  $\gamma$  values of the  
 271 reactions contributing to sulfate and nitrate (R19–R21, R24) are calculated as the  
 272 following equation:

273

$$274 \quad \gamma_i = \begin{cases} \gamma_{low}, RH \in [0, 50\%] \\ \gamma_{low} + (\gamma_{high} - \gamma_{low}) / (RH_{\max} - 0.5) \times (RH - 0.5), RH \in (50\%, RH_{\max}] \\ \gamma_{high}, RH \in (RH_{\max}, 100\%] \end{cases} \quad (2)$$

275

276 where  $i$  represents the reactant for heterogeneous reactions,  $RH_{\max}$  is the RH value at  
 277 which the  $\gamma$  reaches the upper limit, and  $\gamma_{low}$  and  $\gamma_{high}$  are the lower and upper limits of  
 278  $\gamma$  values taken from Table 2 of K. Wang et al. (2012) with one exception for R24.

279 In-situ observations have found significant enhancement of SO<sub>2</sub> oxidation rates  
 280 under wet conditions, indicating possible missing heterogeneous reactions on  
 281 deliquescent particles (G. J. Zheng et al., 2014). However, the coefficients of SO<sub>2</sub>  
 282 uptake by aerosols (R24) are only established for ice surfaces and mineral dust  
 283 particles (Kolb et al., 2010). As the parameterization of heterogeneous reaction of SO<sub>2</sub>  
 284 on soot, organics, and SNA aerosols are not well established yet, we first took the

285 uptake coefficients from K. Wang et al. (2012) and conducted four sensitivity runs,  
286 S1, S2, S3 and S4 by adjusting the uptake coefficients with successive approximation  
287 approach. The parameters and evaluations of the four sensitivity runs are presented in  
288 supplementary information (Table S1 and Fig. S1). The  $\gamma$  values of the lower and  
289 upper limits of SO<sub>2</sub> recommended by K. Wang et al. (2012) are  $1.0 \times 10^{-4}$  and  
290  $2.6 \times 10^{-4}$ , respectively, whereas other works recommended lower  $\gamma$  values for SO<sub>2</sub>,  
291 e.g.,  $4.0 \times 10^{-5}$  in Crowley et al. (2010),  $1.35 \times 10^{-5}$  in Shang et al. (2010), and  
292  $0.6 \times 10^{-5}$  to  $2.45 \times 10^{-4}$  in Wu et al. (2011). We found that using  $\gamma$  in K. Wang et al.  
293 (2012) for R24 (sensitivity run S1) will produce unreasonably high sulfate for this  
294 haze episode. We finally choose the value from S3 in our work, which can best match  
295 observations.

296 We assume the RH<sub>max</sub> of sulfate-related heterogeneous reaction (R24) to be  
297 100%, and that of nitrate-related heterogeneous reactions (R19–R21) to be 70%. This  
298 assumption is made on the basis of the observational result that the SOR increases  
299 when the RH rises from 50% to 100% and the NOR increases when the RH rises from  
300 50% to 70% and then stays stable when the RH continues to increase. The similar  
301 relationship between sulfur (nitrogen) conversion ratios and RH has also been  
302 reported in another pollution episode that occurred in the winter of 2011 in Beijing  
303 (Sun et al., 2013). For other heterogeneous reactions, we use the mean of lower and  
304 upper limit values in the model and assume that they remain constant under different  
305 RHs.

306

### 307 **3. Model Configurations, Simulation Design and Evaluation Protocol**

#### 308 **3.1. Model Configurations and Simulation Design**

309 WRF/CMAQ simulations are performed over East Asia at a horizontal resolution  
310 of  $36 \times 36$  km (see Fig. 2). The simulation period is from 1 to 31 January 2013 with  
311 additional 7 days used as a spin-up period to minimize the influence of initial  
312 conditions.

313 The physics options selected for the WRF simulation are summarized in Table 2.  
314 They are selected based on a number of initial simulations with different option  
315 combinations to ensure the best performance for meteorological predictions against  
316 observations during this episode. The meteorological initial and boundary conditions

317 (ICs and BCs) are based on the National Centers for Environmental Prediction Final  
318 Analysis (NCEP-FNL) reanalysis data. The surface roughness is corrected by  
319 increasing the friction velocity by 1.5 times only in the boundary layer scheme to  
320 reduce the high biases in wind speed (Mass and Ovens, 2010).

321 The configurations and options used in the CMAQ model are summarized in  
322 Table 3. The gas-phase mechanism module is the CB05 gas-phase mechanism with  
323 active chlorine chemistry and updated toluene mechanism of Whitten et al. (2010).  
324 The aqueous-phase chemistry is based on the updated mechanism of the Regional  
325 Acid Deposition Model (RADM) model (Walcek and Taylor, 1986; Chang et al.,  
326 1987). The aerosol mechanism applied in this study is the AERO6 aerosol module.  
327 The photolytic rates are calculated in-line using simulated aerosols and ozone  
328 concentrations. The ICs and BCs are generated from the GEOS-Chem model (Bey et  
329 al., 2001).

330 Anthropogenic emissions for China in 2013 used in this work are derived from  
331 the MEIC model (Multi-resolution Emission Inventory of China,  
332 <http://www.meicmodel.org>). The MEIC model is a dynamic and technology-based  
333 emission model developed by Tsinghua University which estimates anthropogenic  
334 emissions for about 700 emitting sources over China with unified methodology  
335 (Zhang et al., 2007, 2009; Lei et al., 2011a). MEIC model is an update of the bottom-  
336 up emission inventory developed by the same group (Zhang et al., 2007, 2009; Lei et  
337 al., 2011a) with several updates such as unit-based emission data for power plants (S.  
338 W. Wang et al., 2012) and cement plants (Lei et al., 2011b), high-resolution vehicle  
339 emission inventory at county level (B. Zheng et al., 2014), and new NMVOC  
340 mapping approach for different chemical mechanisms (Li et al., 2014). In the MEIC  
341 model, the latest available emission data with real statistics at provincial level is for  
342 2012. In this work, emissions for the year of 2013 are used from the extrapolation of  
343 the 2012 estimates and updated based on brief statistics at country level.

344 Anthropogenic emissions from the other Asian countries and biomass burning  
345 emissions are taken from the MIX emission inventory prepared for the Model Inter-  
346 comparison Study Asia Phase III (MICS-ASIA III). Biogenic emissions are calculated  
347 by the MEGAN v2.1 (Guenther et al., 2012). Sea salt emission and dust emission are  
348 calculated online on the basis of the algorithms developed by Gong (2003) and a  
349 physical-based dust emission algorithm FENGSHA  
350 ([http://www.airqualitymodeling.org/cmaqwiki/index.php?title=CMAQv5.0\\_Windblo](http://www.airqualitymodeling.org/cmaqwiki/index.php?title=CMAQv5.0_Windblo)

351 wn\_Dust), respectively.

352 Using the WRF/CMAQ modeling system, the impacts of heterogeneous  
353 chemistry and the meteorological anomaly of 2013 on the significant production of  
354 sulfate and nitrate aerosols during the January 2013 haze episode are investigated with  
355 three simulations, as shown in Table 4. The simulation Original CMAQ uses the  
356 officially released version of CMAQ v5.0.1. In the simulation Revised CMAQ, nine  
357 important heterogeneous reactions are implemented in the model to explore the effects  
358 of heterogeneous chemistry. To further evaluate the impacts of the 2013  
359 meteorological anomaly on sulfate and nitrate production, another simulation with  
360 revised CMAQ is designed to use the same 2013 emissions but with the WRF  
361 meteorological predictions for 2012 (Revised CMAQ with 2013Emis&2012Met). **The**  
362 **uptake coefficients of heterogeneous chemistry used in the latter two simulations are**  
363 **presented in Table S2 of supplementary information.**

### 364 **3.2. Evaluation Protocol**

365 The model evaluation is performed in terms of domain-wide performance  
366 statistics and site-specific temporal variations. The performance statistics are  
367 conducted following the evaluation protocol of Zhang et al. (2006, 2011). The  
368 statistical parameters include correlation coefficient (R), mean bias (MB), root mean  
369 square error (RMSE), NMB, and normalized mean error (NME).

370 Table 5 summarizes the observational datasets used for model evaluation in this  
371 study. Three observational datasets are used including the meteorological data from  
372 the National Climate Data Center (NCDC), the real-time gaseous and particulate  
373 concentrations in 74 cities from the China National Environmental Monitoring Center  
374 (CNEMC), and hourly concentrations of chemical species of PM<sub>2.5</sub> from the ground-  
375 based measurement at the Tsinghua University site (THU) located in the northwestern  
376 Beijing. The detailed description of these dataset can be found in the supplementary  
377 information.

378

## 379 **4. Results and Discussion**

### 380 **4.1. Evaluation of Meteorological Predictions**

381 Table 6 presents the statistical performances of the meteorological predictions,

382 including temperature at 2 m (T2), RH at 2 m (RH2), wind speed at 10 m (WS10),  
383 wind direction at 10 m (WD10), and daily mean precipitation (Precip). The near-  
384 surface temperature agrees reasonably well with observations with MBs of  $-0.8\text{ }^{\circ}\text{C}$ .  
385 Simulated RH2 agrees well with observations across most of China with an NMB of  
386 9.9% and an MB of 6.7%. WS10 is overpredicted slightly with an NMB of 9.5% and  
387 an MB of  $0.3\text{ m s}^{-1}$  for the 36-km domain. The MB of Precip is 1.1 mm and the NMB  
388 is 58.8% with a relatively poor performance compared with other meteorological  
389 variables. Precip is usually predicted with large biases by meteorological models  
390 (Zhang et al., 2011, 2012; L. T. Wang et al., 2014), indicating the limited capability of  
391 model to accurately reproduce the precipitating processes. The simulated  
392 meteorological variables show generally good agreement with observations, and the  
393 overall performances are consistent with similar work conducted for China using the  
394 Fifth-Generation Penn State/NCAR Mesoscale Model (MM5) or WRF models (Liu et  
395 al., 2010; L. T. Wang et al., 2010, 2014; Zhang et al., 2011; K. Wang et al., 2012; Fu  
396 et al., 2014). The simulated meteorological variables agree well with observations in  
397 terms of temporal variations and magnitudes at the THU site (as shown in Fig. 3),  
398 confirming the reliability of meteorological prediction at location with SNA  
399 observation data.

## 400 4.2. Chemical Predictions of the Original CMAQ at THU Site

### 401 4.2.1 Sulfate, Nitrate and Ammonium

402 **Figure 4** compares the temporal variations of aerosol compositions in January  
403 2013 simulated by the original CMAQ with observation at the THU site, and the  
404 statistical performance of the model were summarized in Table 7. Although the  
405 original CMAQ model only underpredicts  $\text{PM}_{2.5}$  mass concentration by 21.9%, it  
406 significantly underpredicts  $\text{SO}_4^{2-}$ ,  $\text{NO}_3^-$ , and  $\text{NH}_4^+$  concentration with NMBs of  
407  $-54.2\%$ ,  $-40.0\%$ , and  $-58.1\%$ , respectively. The modeled hourly  $\text{PM}_{2.5}$  concentration  
408 shows good agreement with the observations when the  $\text{PM}_{2.5}$  concentration is below  
409  $450\text{ }\mu\text{g m}^{-3}$ . However, the model failed to predict SNA variations during the polluted  
410 days, leading to a large underprediction of total  $\text{PM}_{2.5}$  mass concentration during the  
411 heavy haze episodes when SNA are dominant compositions in total  $\text{PM}_{2.5}$  mass.  
412 **Figure 5a** illustrates the enhancement of SNA in  $\text{PM}_{2.5}$  in haze days in January 2013 at  
413 THU site. The contribution of SNA to total  $\text{PM}_{2.5}$  mass increased from 29.3% to

414 50.3% from clean days to heavily polluted days due to the increased conversion rates  
415 of SO<sub>2</sub> and NO<sub>2</sub> under the haze condition (Sun et al., 2013, 2014), while the original  
416 CMAQ model could not reproduce the dominant contribution of SNA to PM<sub>2.5</sub> for  
417 those episodes, indicating that some mechanisms that might have significant impacts  
418 on SO<sub>4</sub><sup>2-</sup> and NO<sub>3</sub><sup>-</sup> formation during haze episodes are absent in the original CMAQ  
419 model.

420 As discussed in Sect. 2.2, we believe that heterogeneous chemistry played a key  
421 role in sulfate and nitrate production under the haze condition. Nine heterogeneous  
422 reactions have been incorporated into the original CMAQ model to improve the  
423 model capability in reproducing the observed high concentrations of sulfate and  
424 nitrate and study the role of these reactions in the haze pollution. The simulation  
425 results from the revised CMAQ with these heterogeneous reactions are described in  
426 Sect. 4.3.

#### 427 **4.2.2 Carbonaceous Aerosols**

428 As shown in Fig. 4, the original CMAQ model can generally capture the  
429 temporal variation of element carbon at THU site but has a positive bias of 196.2% in  
430 monthly mean concentration, implying large overestimation of element carbon  
431 emissions in the MEIC inventory for urban Beijing area. The MEIC inventory used in  
432 this work is first calculated by province and then allocated to grids by uniformed  
433 spatial proxies across provinces, which may induce significant bias for specific  
434 locations. Coal boilers and stoves have been phased out from Beijing urban areas and  
435 diesel trucks are also prohibited for entering the urban center of Beijing during  
436 daytime. These local policies are not considered in MEIC emission inventory, which  
437 may lead to the overestimation of element carbon emissions in Beijing urban areas.  
438 For organic carbon, the large bias only exists during haze days with mass  
439 concentrations larger than 60 µg m<sup>-3</sup>. As the secondary organic aerosols (SOA)  
440 module used in CMAQ does not include the formation pathways of heterogeneous  
441 reactions involving VOCs and SVOCs, and oligomerization during the haze events  
442 and multi-generations of gas-phase oxidations of semi-VOCs (SVOCs), the  
443 underestimation is probably caused by the underpredictions in SOA.

### 444 4.3. Improvements of SNA Predictions by the Revised CMAQ with 445 Heterogeneous Chemistry

446 **Figure 4** compares the temporal variations of  $\text{PM}_{2.5}$ ,  $\text{SO}_4^{2-}$ ,  $\text{NO}_3^-$ ,  $\text{NH}_4^+$ , OC, and  
447 EC at the THU site simulated by the original and revised CMAQ with observations.  
448 The sulfate and nitrate simulations with heterogeneous chemistry are improved  
449 significantly in terms of both magnitude and temporal variation. In particular, the  
450 significant discrepancies in  $\text{PM}_{2.5}$ ,  $\text{SO}_4^{2-}$ ,  $\text{NO}_3^-$  and  $\text{NH}_4^+$  between the observed and  
451 simulated concentrations during severely polluted days are improved, although a  
452 couple of observed peak values are still not captured well. The synergic improvement  
453 of SNA predictions illustrates the significant role heterogeneous chemistry plays in  
454 the haze pollution events. The revised CMAQ shows better performance with NMBs  
455 of 0.4%, 6.3%, 5.7%, and  $-4.1\%$ , for  $\text{PM}_{2.5}$ ,  $\text{SO}_4^{2-}$ ,  $\text{NO}_3^-$ , and  $\text{NH}_4^+$ , respectively. The  
456 MBs of sulfate and nitrate are reduced, changing from  $-17.8$  to  $2.1 \mu\text{g m}^{-3}$  and from  
457  $-12.3$  to  $1.8 \mu\text{g m}^{-3}$ , respectively. As expected, the simulated level of  $\text{PM}_{2.5}$  is also  
458 improved with MBs changing from  $-40.8$  to  $0.8 \mu\text{g m}^{-3}$ .

459 The revised CMAQ can capture the enhancement of relative contribution of SNA  
460 from clean days to polluted days, as shown in **Fig. 5**. Observations show that the  
461 fractions of SNA increase rapidly to 42.2% and 50.3% on polluted and heavily  
462 polluted days, which are well reproduced by the revised CMAQ with fractions of  
463 49.0% and 52.6%. For comparison, the original CMAQ gives SNA fractions of 32.1%  
464 and 30.8%, which are considerably lower. During polluted and heavily polluted days,  
465 there exist significant discrepancies in SNA percentage contributions between the  
466 original and revised CMAQ, indicating the important role of heterogeneous chemistry  
467 in haze pollution. **It should be noted that the good agreement between the revised  
468 CMAQ and observations is highly dependent on the selections of uptake coefficients,  
469 as discussed in Sect. 2.2. However, all sensitivity runs can reproduce the enhancement  
470 of relative contribution of sulfate in haze days (Fig. S1), implying the importance of  
471 heterogeneous chemistry. Laboratory measurements of uptake coefficients on the  
472 surfaces of mixed and deliquescent aerosols will help to confirm our findings in the  
473 future.**

474 The evolution patterns of SNA simulated by the revised CMAQ are also  
475 generally consistent with other field observations on haze episodes in China, which  
476 confirmed the significance of heterogeneous chemistry in haze formation process over  
477 China. The enhanced SNA contribution in haze days compared to clean days were

478 also observed in other field campaigns, where the heterogeneous chemistry was  
479 attributed as the most probable pathway of observed abrupt increases in SNA aerosols  
480 as the oxidation rates of gas-phase and aqueous-phase chemistry were too slow (X. J.  
481 Zhao et al., 2013; Ji et al., 2014; Quan et al., 2014; Y. S. Wang et al., 2014). Strong  
482 correlations between RH and sulfur and nitrogen oxidation ratios (SOR and NOR)  
483 were found during haze episodes (X. Wang et al., 2012; Y. S. Wang et al., 2014; Sun  
484 et al., 2014; G. J. Zheng et al., 2014) with sharp increase of SOR and NOR when RH  
485 exceeds 50%, lending support to our assumptions in the revised CMAQ.

486 The revised CMAQ gives very similar OC and EC predictions as original  
487 CMAQ, with large underpredictions in OC during the haze episodes but  
488 overpredictions in EC throughout the simulation period for the reasons discussed  
489 previously in Sect. 4.2.2. The percent contributions for EC and OIN are also slightly  
490 decreased especially in the polluted and heavily polluted days. This is because the  
491 mode-averaging particle diameter is larger due to the enhanced formation of SNA  
492 when the heterogeneous reactions are included. The particle settling velocity is  
493 increased and thus dry deposition rates are larger, which helps reduce the  
494 overpredictions of these species.

#### 495 **4.4. Domain-wide Impact from the Implementation of Heterogeneous** 496 **Chemistry**

497 The simulation results with and without heterogeneous chemistry are compared  
498 over the whole domain to evaluate the impact of heterogeneous reactions during the  
499 January 2013 haze episode. Table 8 summarizes the statistical performance for surface  
500 concentrations of CO, NO<sub>2</sub>, SO<sub>2</sub>, PM<sub>2.5</sub>, and PM<sub>10</sub> from the simulation with original  
501 CMAQ and revised CMAQ for 74 cities in China. The original CMAQ model can  
502 generally reproduce the concentrations of aerosol and gaseous pollutants over the  
503 whole domain. The model underpredicts the concentrations of CO and PM<sub>10</sub> with  
504 NMBs of -20.6% and -11.2%, respectively, and overpredicts those of SO<sub>2</sub>, NO<sub>2</sub>, and  
505 PM<sub>2.5</sub> with NMBs of 51.2%, 13.4%, and 8.1%, respectively. As expected, the  
506 overpredictions in SO<sub>2</sub> and NO<sub>2</sub> are improved in the revised CMAQ model because  
507 the added heterogeneous reactions enhance their conversions to sulfate and nitrate.  
508 The positive biases of SO<sub>2</sub> and NO<sub>2</sub> are reduced from 51.2% to 38.5% and 13.4% to  
509 11.2%. We further found that high NMB in SO<sub>2</sub> prediction is mainly contributed by  
510 provincial capital cities. As the most developed cities within China, the provincial  
511 capital cities tend to prohibit coal use in urban areas or use high-quality coal with low



512 sulfur content, which has not been accurately represented in regional emission  
513 inventories which are compiled at the provincial level. As a result, SO<sub>2</sub> emissions  
514 from those capital cities may have been overestimated.

515 **Figure 6** illustrates the concentration of SNA and PM<sub>2.5</sub> simulated by the original  
516 and revised CMAQ and **Fig. 7 further explores the difference in heavily polluted**  
517 **regions**. Heterogeneous chemistry enhances SNA concentrations significantly in the  
518 most polluted regions in China (the Northeast Plain (NP), NCP, Middle-Lower  
519 Yangtze Plain (MLYP), and Sichuan Basin (SB)), leading to the increased PM<sub>2.5</sub>  
520 concentration over those regions. In southern China (e.g., the Pearl River Delta  
521 (PRD)), sulfate concentration is still increased but nitrate concentration is decreased  
522 by 5–20 μg m<sup>-3</sup>, resulting in a reduction of PM<sub>2.5</sub> concentration by 10–20 μg m<sup>-3</sup>. The  
523 contrasting responses to heterogeneous chemistry in different regions are because of  
524 the complex thermodynamic processes of SNA formation, which differ greatly under  
525 NH<sub>3</sub>-rich and NH<sub>3</sub>-poor conditions. The polluted regions listed above (NP, NCP,  
526 MLYP, and SB) are all NH<sub>3</sub>-rich regions (Wang et al., 2011; **B. Zhao et al., 2013**), as  
527 **shown in Fig. 7a**, which comprise 24.5% land areas in China but contribute to 47.4%  
528 cultivated lands (National Bureau of Statistics, 2013) and 48.3% NH<sub>3</sub> emissions  
529 (derived from the MEIC model). The abundant NH<sub>3</sub> emissions provide sufficient  
530 amounts of ammonium to neutralize the increased amounts of sulfate and nitrate  
531 formed through heterogeneous chemistry; therefore, the total amount of PM<sub>2.5</sub> in these  
532 regions increases with enhancement of both sulfate and nitrate. It causes the positive  
533 bias of simulated PM<sub>2.5</sub> to be larger in the NH<sub>3</sub>-rich regions, mainly contributed by the  
534 overpredictions of EC and OIN. In southern China, which is an NH<sub>3</sub>-poor region in  
535 January (Wang et al., 2011), sulfate and nitrate compete for ammonium and the  
536 formation of ammonium sulfate occurs first owing to its more thermodynamically  
537 stable characteristics, increased levels of sulfate would thus lead to a decrease of  
538 nitrate. This phenomenon could even lead to the decrease in the total concentration of  
539 PM<sub>2.5</sub>, because to neutralize with the same amount of ammonium, the mass of sulfate  
540 required is smaller than that of nitrate.

#### 541 **4.5. Impact of Meteorology in 2013 on SNA Production**

542 The haze episode in January 2013 was the most serious pollution event in recent  
543 years. Why it should happen in 2013 but not in other years is an intriguing question.  
544 Emissions of SO<sub>2</sub>, NO<sub>x</sub>, and PM<sub>2.5</sub> kept stable during 2011-2013 (**derived from the**

545 MEIC model), indicating that emissions are not the critical driving force. The  
546 anomalous meteorological conditions (low temperature, high RH, and low wind  
547 speed) in January 2013 are identified as the key influence factor of haze formation by  
548 affecting radiation, horizontal transport, vertical mixing, and the atmospheric reaction  
549 rates of air pollutants (Ding and Liu, 2014; Z. F. Wang et al., 2014). As described in  
550 Sect. 2.2, meteorological conditions (specifically RH) can affect heterogeneous  
551 chemistry by increasing the uptake coefficients of gases. In this section, the impact of  
552 the 2013 meteorological conditions on the production of sulfate and nitrate is  
553 evaluated using the revised CMAQ with heterogeneous chemistry.

554 The meteorological conditions of 2012 are selected to represent typical weather  
555 conditions because they were very close to the 10-year average climatology  
556 conditions with regard to temperature, RH, wind speed, and sea level pressure (data  
557 derived from <http://cdc.cma.gov.cn>) in the region of the NCP. Figure 8 illustrates the  
558 spatial distributions of the monthly mean temperature, RH, PM<sub>2.5</sub>, sulfate, and nitrate  
559 simulated by the revised CMAQ with the meteorological fields of 2012 and 2013. The  
560 simulated temperature of 2013 in North and East China is 2–3 °C lower than that in  
561 2012 and the simulated RH is 5–25% higher. High RH promotes heterogeneous  
562 conversions to generate more sulfate and nitrate and therefore, to increase the total  
563 concentration of PM<sub>2.5</sub>. Significant differences in RH occur in the NCP region, where  
564 increases by 15–30% in RH correspond to increases of PM<sub>2.5</sub> concentration by 70–150  
565 μg m<sup>-3</sup>.

566 Traditional chemistry mechanisms play a relatively small role during haze  
567 formation because of the low solar radiation and low temperature conditions, and few  
568 precipitating clouds, whereas heterogeneous chemistry mechanisms are enhanced by  
569 the extremely high RH, which leads to the significant production of sulfate and nitrate  
570 aerosols. This provides a perspective to understand how adverse meteorological  
571 conditions can affect air quality through reaction pathways that are sensitive to  
572 specific meteorological variables. The meteorological anomaly of 2013 occurred not  
573 only for temperature and RH, but also for other variables, for example, the shallower  
574 PBL and lower wind speed than a typical year. The abnormal changes in these  
575 variables also have adverse effects on haze pollution. For example, the height of the  
576 PBL across China in 2013 was about 200 m lower than in 2012, which could weaken  
577 and confine the vertical mixing of pollutants and thus, aggravate surface pollution.  
578 Researches on the impact of these factors have been reported in other studies (e.g., Z.

579 F. Wang et al., 2014; R. H. Zhang et al., 2014).

580

## 581 5. Summary and Conclusions

582 In this work, the WRF/CMAQ has been applied to simulate the January 2013  
583 haze episode in China and evaluate the role heterogeneous chemistry played in the  
584 formation of sulfate and nitrate during this episode. The simulations with the original  
585 and the revised CMAQ are performed and evaluated. In the simulation by original  
586 CMAQ,  $\text{PM}_{2.5}$ ,  $\text{SO}_4^{2-}$ ,  $\text{NO}_3^-$ , and  $\text{NH}_4^+$  are underpredicted with NMBs of  $-21.9\%$ ,  
587  $-54.2\%$ ,  $-40.0\%$ , and  $-58.1\%$ , respectively, at the THU site. The incorporation of  
588 additional heterogeneous chemistry into CMAQ v5.0.1 significantly improves the  
589 model's capability in reproducing sulfate and nitrate concentrations, which are the  
590 most important  $\text{PM}_{2.5}$  compositions on polluted haze days. The revised CMAQ shows  
591 better performances with NMBs of  $0.4\%$ ,  $6.3\%$ ,  $5.7\%$ , and  $-4.1\%$ , for  $\text{PM}_{2.5}$ ,  $\text{SO}_4^{2-}$ ,  
592  $\text{NO}_3^-$ , and  $\text{NH}_4^+$ , respectively, at the THU site. The MBs of sulfate and nitrate are  
593 reduced, changing from  $-17.8$  to  $2.1 \mu\text{g m}^{-3}$  and from  $-12.3$  to  $1.8 \mu\text{g m}^{-3}$ ,  
594 respectively. The revised CMAQ with enhanced heterogeneous chemistry not only  
595 captures the magnitude and temporal variation of SNA concentrations, but also  
596 reproduces the enhancement of SNA compositions from clean air to polluted haze  
597 days, both of which indicate the significantly improved capability of the revised  
598 model for haze studies. The revised CMAQ model is then used to evaluate the impact  
599 of both heterogeneous chemistry on haze formation during January 2013 and of the  
600 meteorological anomaly in 2013 on heterogeneous generation of sulfate and nitrate.

601 Compared with previous studies focusing on the haze episode of January 2013,  
602 this work provides a unique method to explore the formation mechanisms of severe  
603 haze by evaluating initial application of the original CMAQ, identifying missing  
604 heterogeneous chemistry based on model performance, and then incorporating those  
605 missing reactions into CMAQ. It thus provides a mechanistic level of understanding  
606 of the formation mechanism of the severe regional haze pollution episode.

607 This study has several limitations. First, heterogeneous chemistry is implemented  
608 into CMAQ with several assumptions. For example, a pseudo-first-order rate constant  
609 is assumed for those reactions and the gas uptake coefficients are assumed to be  
610 linearly correlated with RH. Those simplified treatments neglect the effects of  
611 complex aerosol compositions and surface uptake, diffusion, and coating and reaction  
612 processes, which could inevitably introduce errors and uncertainties in this work (Wei,

613 2010). As a consequence, for example, while the peak concentrations of sulfate and  
614 nitrate during the haze pollution event were sharp and occurred during a narrow time  
615 window, the revised CMAQ predicts lower and wider spread concentrations. The RH-  
616 dependent parameterization of uptake coefficients derived in this work can be refined  
617 to consider additional factors, such as temperature, aerosol compositions, amounts of  
618 metal catalyst, and surface conditions. In addition, some newly reported  
619 heterogeneous reactions, such as SO<sub>2</sub> oxidation promoted by NO<sub>x</sub> (He et al., 2014)  
620 and OH derived from heterogeneous ClNO<sub>2</sub> production (Sarwar et al., 2014) can  
621 enhance SNA but have not yet been included in this work which should be  
622 incorporated into CMAQ in the future.

623 Second, there is a lack of sufficient site-specific hourly data for PM<sub>2.5</sub> and its  
624 composition, which are crucial to the model evaluation and improvement. For  
625 example, we do not have observation data to evaluate the predicted Fe and Mn in  
626 aerosols. The underprediction of Fe and Mn can contribute to the underprediction of  
627 sulfate, because the metal catalysis pathway is important for sulfate formation.  
628 Although this might not be a critical issue as the model can well predict sulfate  
629 concentration in clean days and the metal catalysis pathway is not dependent on  
630 relative humidity (Seinfeld and Pandis, 2006), more observed data for compositions  
631 of PM<sub>2.5</sub> is needed to comprehensively evaluate the model.

632 Finally, the WRF/CMAQ system used in this work is not online-coupled, which  
633 does not account for the feedbacks of chemistry and aerosol into meteorology. J.  
634 Wang et al. (2014) simulated the same episode using the online-coupled CMAQ and  
635 found that including aerosol feedback can increase total aerosol loadings during haze  
636 conditions and improve model performance, but lead to larger enhancement of  
637 primary aerosols than secondary aerosols, which is opposite to the observations.  
638 Online-coupled models with improved chemistry should be developed in the future.  
639 Addressing these uncertainties requires an integration of field studies, laboratory  
640 experiments, and modeling work by the entire community.

641

## 642 **Acknowledgements**

643 The work was supported by China's National Basic Research Program  
644 (2010CB951803 and 2014CB441301), the National Science Foundation of China  
645 (41222036 and 21221004), the Japan International Cooperation Agency, and the U.S.

646 DOE climate modeling programs (DESC0006695) at NCSU, U.S.A. We thank the  
647 constructive comments from Dr. Muller and two anonymous reviewers.

648 **References**

- 649 American Lung Association: 2005 research highlights: health effects of particulate  
650 matter and ozone air pollution, [http://www.northeastdiesel.org/pdf/ALA-05-health-](http://www.northeastdiesel.org/pdf/ALA-05-health-studies-biblio.pdf)  
651 [studies-biblio.pdf](http://www.northeastdiesel.org/pdf/ALA-05-health-studies-biblio.pdf) (last access: June 2014), 2006.
- 652
- 653 Bey, I., Jacob, D. J., Yantosca, R. M., Logan, J. A., Field, B. D., Fiore, A. M., Li, Q.,  
654 Liu, H. Y., Mickley, L. J., and Schultz, M. G.: Global modeling of tropospheric  
655 chemistry with assimilated meteorology: Model description and evaluation, *J.*  
656 *Geophys. Res.-Atmos.*, 106, 23073–23095, doi: 10.1029/2001jd000807, 2001.
- 657
- 658 Chang, J. S., Brost, R. A., Isaksen, I. S. A., Madronich, S., Middleton, P., Stockwell,  
659 W. R., and Walcek, C. J.: A three-dimensional Eulerian acid deposition model:  
660 Physical concepts and formulation, *J. Geophys. Res.-Atmos.*, 92, 14681–14700, doi:  
661 10.1029/JD092iD12p14681, 1987.
- 662
- 663 Chang, W. L., Bhave, P. V., Brown, S. S., Riemer, N., Stutz, J., and Dabdub, D.:  
664 Heterogeneous Atmospheric Chemistry, Ambient Measurements, and Model  
665 Calculations of N<sub>2</sub>O<sub>5</sub>: A Review, *Aerosol. Sci. Tech.*, 45, 665–695, doi:  
666 10.1080/02786826.2010.551672, 2011.
- 667
- 668 Chou, M.-D., Suarez, M. J., Ho, C.-H., Yan, M. M. H., and Lee, K.-T.:  
669 Parameterizations for Cloud Overlapping and Shortwave Single-Scattering Properties  
670 for Use in General Circulation and Cloud Ensemble Models, *J. Climate*, 11, 202–214,  
671 doi: 10.1175/1520-0442(1998)011<0202:pfcoas>2.0.co;2, 1998.
- 672
- 673 Crowley, J. N., Ammann, M., Cox, R. A., Hynes, R. G., Jenkin, M. E., Mellouki, A.,  
674 Rossi, M. J., Troe, J., and Wallington, T. J.: Evaluated kinetic and photochemical data  
675 for atmospheric chemistry: Volume V – heterogeneous reactions on solid substrates,  
676 *Atmos. Chem. Phys.*, 10, 9059–9223, doi: 10.5194/acp-10-9059-2010, 2010.
- 677
- 678 Dentener, F. J., Carmichael, G. R., Zhang, Y., Lelieveld, J., and Crutzen, P. J.: Role of  
679 mineral aerosol as a reactive surface in the global troposphere, *J. Geophys. Res.-*  
680 *Atmos.*, 101, 22869–22889, doi: 10.1029/96jd01818, 1996.
- 681
- 682 Ding, Y. H., and Liu, Y. J.: Analysis of long-term variations of fog and haze in China  
683 in recent 50 years and their relations with atmospheric humidity, *Sci. China-Earth*  
684 *Sci.*, 57, 36–46, doi: 10.1007/s11430-013-4792-1, 2014.
- 685
- 686 Fountoukis, C., and Nenes, A.: ISORROPIA II: a computationally efficient  
687 thermodynamic equilibrium model for K<sup>+</sup> - Ca<sup>2+</sup> - Mg<sup>2+</sup> - NH<sub>4</sub><sup>+</sup> - Na<sup>+</sup> - SO<sub>4</sub><sup>2-</sup> - NO<sub>3</sub><sup>-</sup> -  
688 Cl<sup>-</sup> - H<sub>2</sub>O aerosols, *Atmos. Chem. Phys.*, 7, 4639–4659, doi: 10.5194/acp-7-4639-  
689 2007, 2007.
- 690

691 Fu, X., Wang, S. X., Cheng, Z., Xing, J., Zhao, B., Wang, J. D., and Hao, J. M.:  
692 Source, transport and impacts of a heavy dust event in the Yangtze River Delta, China,  
693 in 2011, *Atmos. Chem. Phys.*, 14, 1239–1254, doi: 10.5194/acp-14-1239-2014, 2014.  
694

695 Gong, S. L.: A parameterization of sea-salt aerosol source function for sub- and super-  
696 micron particles, *Global Biogeochem. Cy.*, 17, 1097, doi: 10.1029/2003gb002079,  
697 2003.  
698

699 Guenther, A. B., Jiang, X., Heald, C. L., Sakulyanontvittaya, T., Duhl, T., Emmons, L.  
700 K., and Wang, X.: The Model of Emissions of Gases and Aerosols from Nature  
701 version 2.1 (MEGAN2.1): an extended and updated framework for modeling biogenic  
702 emissions, *Geosci. Model Dev.*, 5, 1471–1492, doi: 10.5194/gmd-5-1471-2012, 2012.  
703

704 He, H., Wang, Y., Ma, Q., Ma, J., Chu, B., Ji, D., Tang, G., Liu, C., Zhang, H., and  
705 Hao, J.: Mineral dust and NO<sub>x</sub> promote the conversion of SO<sub>2</sub> to sulfate in heavy  
706 pollution days, *Sci. Rep.*, 4, 4172, doi: 10.1038/srep04172, 2014.  
707

708 Henson, B. F., Wilson, K. R., and Robinson, J. M.: A physical adsorption model of the  
709 dependence of ClONO<sub>2</sub> heterogeneous reactions on relative humidity, *Geophys. Res.*  
710 *Lett.*, 23, 1021–1024, doi: 10.1029/96gl00871, 1996.  
711

712 Hong, S. Y. and Lim, J. O. J.: The WRF Single-Moment 6-Class Microphysics  
713 Scheme (WSM6), *J. Korean Meteor. Soc.*, 42, 129–151,  
714 [http://www2.mmm.ucar.edu/wrf/users/docs/WSM6-hong\\_and\\_lim\\_JKMS.pdf](http://www2.mmm.ucar.edu/wrf/users/docs/WSM6-hong_and_lim_JKMS.pdf) (last  
715 access: June 2014), 2006.  
716

717 Jacob, D. J.: Heterogeneous chemistry and tropospheric ozone, *Atmos. Environ.*, 34,  
718 2131–2159, doi: 10.1016/S1352-2310(99)00462-8, 2000.  
719

720 Ji, D., Li, L., Wang, Y., Zhang, J., Cheng, M., Sun, Y., Liu, Z., Wang, L., Tang, G., Hu,  
721 B., Chao, N., Wen, T., and Miao, H.: The heaviest particulate air-pollution episodes  
722 occurred in northern China in January, 2013: Insights gained from observation,  
723 *Atmos. Environ.*, 92, 546–556, doi:10.1016/j.atmosenv.2014.04.048, 2014.  
724

725 Kain, J. S.: The Kain–Fritsch Convective Parameterization: An Update, *J. Appl.*  
726 *Meteorol.*, 43, 170–181, doi: 10.1175/1520-0450(2004)043<0170:tkcpau>2.0.co;2,  
727 2004.  
728

729 Kolb, C. E., Cox, R. A., Abbatt, J. P. D., Ammann, M., Davis, E. J., Donaldson, D. J.,  
730 Garrett, B. C., George, C., Griffiths, P. T., Hanson, D. R., Kulmala, M.,  
731 McFiggans, G., Pöschl, U., Riipinen, I., Rossi, M. J., Rudich, Y., Wagner, P. E.,  
732 Winkler, P. M., Worsnop, D. R., and O' Dowd, C. D.: An overview of current issues  
733 in the uptake of atmospheric trace gases by aerosols and clouds, *Atmos. Chem. Phys.*,  
734 10, 10561–10605, doi:10.5194/acp-10-10561-2010, 2010.

735  
736 Lammel, G., and Leip, A.: Formation of Nitrate and Sulfate in the Plume of Berlin,  
737 Environ. Sci. Pollut. R., 12, 213–220, doi: 10.1065/espr2005.03.240, 2005.  
738  
739 Lei, Y., Zhang, Q., He, K. B., and Streets, D. G.: Primary anthropogenic aerosol  
740 emission trends for China, 1990–2005, Atmos. Chem. Phys., 11, 931–954, doi:  
741 10.5194/acp-11-931-2011, 2011a.  
742  
743 Lei, Y., Zhang, Q., Nielsen, C., and He, K.: An inventory of primary air pollutants and  
744 CO<sub>2</sub> emissions from cement production in China, 1990–2020, Atmos. Environ., 45,  
745 147–154, doi: 10.1016/j.atmosenv.2010.09.034, 2011b.  
746  
747 Li, M., Zhang, Q., Streets, D. G., He, K. B., Cheng, Y. F., Emmons, L. K., Huo, H.,  
748 Kang, S. C., Lu, Z., Shao, M., Su, H., Yu, X., and Zhang, Y.: Mapping Asian  
749 anthropogenic emissions of non-methane volatile organic compounds to multiple  
750 chemical mechanisms, Atmos. Chem. Phys., 14, 5617–5638, doi:10.5194/acp-14-  
751 5617-2014, 2014.  
752  
753 Li, W., and Shao, L.: Transmission electron microscopy study of aerosol particles  
754 from the brown hazes in northern China, J. Geophys. Res.-Atmos., 114, D09302, doi:  
755 10.1029/2008jd011285, 2009.  
756  
757 Li, W., and Shao, L.: Characterization of mineral particles in winter fog of Beijing  
758 analyzed by TEM and SEM, Environ. Monit. Assess., 161, 565–573, doi:  
759 10.1007/s10661-009-0768-1, 2010.  
760  
761 Li, W., Zhou, S., Wang, X., Xu, Z., Yuan, C., Yu, Y., Zhang, Q., and Wang, W.:  
762 Integrated evaluation of aerosols from regional brown hazes over northern China in  
763 winter: Concentrations, sources, transformation, and mixing states, J. Geophys. Res.-  
764 Atmos., 116, D09301, doi: 10.1029/2010jd015099, 2011.  
765  
766 Li, Z., Xia, X., Cribb, M., Mi, W., Holben, B., Wang, P., Chen, H., Tsay, S.-C., Eck, T.  
767 F., Zhao, F., Dutton, E. G., and Dickerson, R. E.: Aerosol optical properties and their  
768 radiative effects in northern China, J. Geophys. Res.-Atmos., 112, D22S01, doi:  
769 10.1029/2006jd007382, 2007.  
770  
771 Liu, X.-H., Zhang, Y., Cheng, S.-H., Xing, J., Zhang, Q., Streets, D. G., Jang, C.,  
772 Wang, W.-X., and Hao, J.-M.: Understanding of regional air pollution over China  
773 using CMAQ, part I performance evaluation and seasonal variation, Atmos. Environ.,  
774 44, 2415–2426, doi: 10.1016/j.atmosenv.2010.03.035, 2010.  
775  
776 Liu, Y., Gibson, Cain, Wang, H., Grassian, and Laskin, A.: Kinetics of Heterogeneous  
777 Reaction of CaCO<sub>3</sub> Particles with Gaseous HNO<sub>3</sub> over a Wide Range of Humidity, J.  
778 Phys. Chem. A, 112, 1561–1571, doi: 10.1021/jp076169h, 2008.



779

780 Mass, C., and Ovens, D.: WRF Model Physics: Progress, Problems, and Perhaps  
781 Some Solutions, The 11<sup>th</sup> WRF Users' Workshop, 21–25 June, NCAR Center Green  
782 Campus,

783 [http://www.mmm.ucar.edu/wrf/users/workshops/WS2010/presentations/session%204/  
784 4-1\\_WRFworkshop2010Final.pdf](http://www.mmm.ucar.edu/wrf/users/workshops/WS2010/presentations/session%204/4-1_WRFworkshop2010Final.pdf) (last access: June 2014), 2010.

785

786 McNaughton, C. S., Clarke, A. D., Kapustin, V., Shinozuka, Y., Howell, S. G.,  
787 Anderson, B. E., Winstead, E., Dibb, J., Scheuer, E., Cohen, R. C., Wooldridge, P.,  
788 Perring, A., Huey, L. G., Kim, S., Jimenez, J. L., Dunlea, E. J., DeCarlo, P. F.,  
789 Wennberg, P. O., Crouse, J. D., Weinheimer, A. J., and Flocke, F.: Observations of  
790 heterogeneous reactions between Asian pollution and mineral dust over the Eastern  
791 North Pacific during INTEX-B, *Atmos. Chem. Phys.*, 9, 8283–8308, doi:  
792 10.5194/acp-9-8283-2009, 2009.

793

794 Mercado, L. M., Bellouin, N., Sitch, S., Boucher, O., Huntingford, C., Wild, M., and  
795 Cox, P. M.: Impact of changes in diffuse radiation on the global land carbon sink,  
796 *Nature*, 458, 1014–1017, doi: 10.1038/nature07949, 2009.

797

798 Mlawer, E. J., Taubman, S. J., Brown, P. D., Iacono, M. J., and Clough, S. A.:  
799 Radiative transfer for inhomogeneous atmospheres: RRTM, a validated correlated-k  
800 model for the longwave, *J. Geophys. Res.-Atmos.*, 102, 16663–16682, doi:  
801 10.1029/97jd00237, 1997.

802

803 Mogili, P. K., Kleiber, P. D., Young, M. A., and Grassian, V. H.: N<sub>2</sub>O<sub>5</sub> hydrolysis on  
804 the components of mineral dust and sea salt aerosol: Comparison study in an  
805 environmental aerosol reaction chamber, *Atmos. Environ.*, 40, 7401–7408, doi:  
806 10.1016/j.atmosenv.2006.06.048, 2006.

807

808 National Bureau of Statistics: China Statistical Yearbook 2013, China Statistics Press,  
809 Beijing, 2013.

810

811 Peckhaus, A., Grass, S., Treuel, L., and Zellner, R.: Deliquescence and Efflorescence  
812 Behavior of Ternary Inorganic/Organic/Water Aerosol Particles, *J. Phys. Chem. A*,  
813 116, 6199–6210, doi: 10.1021/jp211522t, 2012.

814

815 Pleim, J. E.: A Combined Local and Nonlocal Closure Model for the Atmospheric  
816 Boundary Layer. Part I: Model Description and Testing, *J. Appl. Meteorol. Clim.*, 46,  
817 1383–1395, doi: 10.1175/jam2539.1, 2007.

818

819 Quan, J., Tie, X., Zhang, Q., Liu, Q., Li, X., Gao, Y., and Zhao, D.: Characteristics of  
820 heavy aerosol pollution during the 2012–2013 winter in Beijing, China, *Atmos.*  
821 *Environ.*, 88, 83–89, doi: 10.1016/j.atmosenv.2014.01.058, 2014.

822

823 Ravishankara, A. R.: Heterogeneous and Multiphase Chemistry in the Troposphere,  
824 Science, 276, 1058–1065, doi: 10.1126/science.276.5315.1058, 1997.  
825

826 Reid, J. P., and Sayer, R. M.: Heterogeneous atmospheric aerosol chemistry:  
827 laboratory studies of chemistry on water droplets, Chem. Soc. Rev., 32, 70–79, doi:  
828 10.1039/b204463n, 2003.  
829

830 Sarwar, G., Simon, H., Xing, J., and Mathur, R.: Importance of tropospheric ClNO<sub>2</sub>  
831 chemistry across the Northern Hemisphere, Geophys. Res. Lett., 41, 4050–4058, doi:  
832 10.1002/2014GL059962, 2014.  
833

834 Schumann, U., and Huntrieser, H.: The global lightning-induced nitrogen oxides  
835 source, Atmos. Chem. Phys., 7, 3823–3907, doi: 10.5194/acp-7-3823-2007, 2007.  
836

837 Seinfeld, J. H. and Pandis, S. N.: Atmospheric chemistry and physics: from air  
838 pollution to climate change. Wiley-Interscience, New York, 2006.  
839

840 Seinfeld, J. H., Carmichael, G. R., Arimoto, R., Conant, W. C., Brechtel, F. J., Bates,  
841 T. S., Cahill, T. A., Clarke, A. D., Doherty, S. J., Flatau, P. J., Huebert, B. J., Kim, J.,  
842 Markowicz, K. M., Quinn, P. K., Russell, L. M., Russell, P. B., Shimizu, A.,  
843 Shinzuka, Y., Song, C. H., Tang, Y., Uno, I., Vogelmann, A. M., Weber, R. J., Woo,  
844 J.-H., and Zhang, X. Y.: ACE-ASIA: Regional Climatic and Atmospheric Chemical  
845 Effects of Asian Dust and Pollution, B. Am. Meteorol. Soc., 85, 367–380, doi:  
846 10.1175/bams-85-3-367, 2004.  
847

848 Shang, J., Li, J., and Zhu, T.: Heterogeneous reaction of SO<sub>2</sub> on TiO<sub>2</sub> particles, Sci.  
849 China Chem., 53, 2637–2643, doi: 10.1007/s11426-010-4160-3, 2010.  
850

851 Song, C. H., and Carmichael, G. R.: A three-dimensional modeling investigation of  
852 the evolution processes of dust and sea-salt particles in east Asia, J. Geophys. Res.-  
853 Atmos., 106, 18131–18154, doi: 10.1029/2000jd900352, 2001.  
854

855 Stutz, J., Alicke, B., Ackermann, R., Geyer, A., Wang, S., White, A. B., Williams, E.  
856 J., Spicer, C. W., and Fast, J. D.: Relative humidity dependence of HONO chemistry  
857 in urban areas, J. Geophys. Res.-Atmos., 109, D03307, doi: 10.1029/2003jd004135,  
858 2004.  
859

860 Sun, Y., Zhuang, G., Tang, A., Wang, Y., and An, Z.: Chemical Characteristics of  
861 PM<sub>2.5</sub> and PM<sub>10</sub> in Haze–Fog Episodes in Beijing, Environ. Sci. Technol., 40, 3148–  
862 3155, doi: 10.1021/es051533g, 2006.  
863

864 Sun, Y., Wang, Z., Fu, P., Jiang, Q., Yang, T., Li, J., and Ge, X.: The impact of relative  
865 humidity on aerosol composition and evolution processes during wintertime in  
866 Beijing, China, Atmos. Environ., 77, 927–934, doi: 10.1016/j.atmosenv.2013.06.019,

867 2013.  
868  
869 Sun, Y., Jiang, Q., Wang, Z., Fu, P., Li, J., Yang, T., and Yin, Y.: Investigation of the  
870 Sources and Evolution Processes of Severe Haze Pollution in Beijing in January 2013,  
871 *J. Geophys. Res.-Atmos.*, 119, 4380–4398, doi:10.1002/2014jd021641, 2014.  
872  
873 Usher, C. R., Michel, A. E., and Grassian, V. H.: Reactions on Mineral Dust, *Chem.*  
874 *Rev.*, 103, 4883–4940, doi: 10.1021/cr020657y, 2003.  
875  
876 Walcek, C. J., and Taylor, G. R.: A Theoretical Method for Computing Vertical  
877 Distributions of Acidity and Sulfate Production within Cumulus Clouds, *J. Atmos.*  
878 *Sci.*, 43, 339–355, doi: 10.1175/1520-0469(1986)043<0339:atmfvcv>2.0.co;2, 1986.  
879  
880 Wang, J., Wang, S., Jiang, J., Ding, A., Zheng, M., Zhao, B., Wong, D. C., Zhou, W.,  
881 Zheng, G., Wang, L., Pleim, J. E., and Hao, J.: Impact of aerosol–meteorology  
882 interactions on fine particle pollution during China’s severe haze episode in January  
883 2013, *Environ. Res. Lett.*, 9, doi: 10.1088/1748-9326/9/9/094002, 2014.  
884  
885 Wang, K., Zhang, Y., Nenes, A., and Fountoukis, C.: Implementation of dust emission  
886 and chemistry into the Community Multiscale Air Quality modeling system and initial  
887 application to an Asian dust storm episode, *Atmos. Chem. Phys.*, 12, 10209–10237,  
888 doi: 10.5194/acp-12-10209-2012, 2012.  
889  
890 Wang, L. T., Jang, C., Zhang, Y., Wang, K., Zhang, Q., Streets, D., Fu, J., Lei, Y.,  
891 Schreifels, J., He, K., Hao, J., Lam, Y.-F., Lin, J., Meskhidze, N., Voorhees, S., Evarts,  
892 D., and Phillips, S.: Assessment of air quality benefits from national air pollution  
893 control policies in China. Part I: Background, emission scenarios and evaluation of  
894 meteorological predictions, *Atmos. Environ.*, 44, 3442–3448, doi:  
895 10.1016/j.atmosenv.2010.05.051, 2010.  
896  
897 Wang, L. T., Wei, Z., Yang, J., Zhang, Y., Zhang, F. F., Su, J., Meng, C. C., and Zhang,  
898 Q.: The 2013 severe haze over southern Hebei, China: model evaluation, source  
899 apportionment, and policy implications, *Atmos. Chem. Phys.*, 14, 3151–3173,  
900 doi:10.5194/acp-14-3151-2014, 2014.  
901  
902 Wang, S., Xing, J., Jang, C., Zhu, Y., Fu, J. S., and Hao, J.: Impact Assessment of  
903 Ammonia Emissions on Inorganic Aerosols in East China Using Response Surface  
904 Modeling Technique, *Environ. Sci. Technol.*, 45, 9293–9300, doi:  
905 10.1021/es2022347, 2011.  
906  
907 Wang, S. W., Zhang, Q., Streets, D. G., He, K. B., Martin, R. V., Lamsal, L. N., Chen,  
908 D., Lei, Y., and Lu, Z.: Growth in NO<sub>x</sub> emissions from power plants in China:  
909 bottom-up estimates and satellite observations, *Atmos. Chem. Phys.*, 12, 4429–4447,  
910 doi: 10.5194/acp-12-4429-2012, 2012.

911  
912 Wang, X., Wang, W., Yang, L., Gao, X., Nie, W., Yu, Y., Xu, P., Zhou, Y., and Wang,  
913 Z.: The secondary formation of inorganic aerosols in the droplet mode through  
914 heterogeneous aqueous reactions under haze conditions, *Atmos. Environ.*, 63, 68–76,  
915 doi: 10.1016/j.atmosenv.2012.09.029, 2012.

916  
917 Wang, Y., Zhuang, G., Sun, Y., and An, Z.: The variation of characteristics and  
918 formation mechanisms of aerosols in dust, haze, and clear days in Beijing, *Atmos.*  
919 *Environ.*, 40, 6579–6591, doi: 10.1016/j.atmosenv.2006.05.066, 2006.

920  
921 Wang, Y. S., Yao, L., Wang, L. L., Liu, Z. R., Ji, D. S., Tang, G. Q., Zhang, J. K., Sun,  
922 Y., Hu, B., and Xin, J. Y.: Mechanism for the formation of the January 2013 heavy  
923 haze pollution episode over central and eastern China, *Sci. China-Earth Sci.*, 57, 14–  
924 25, doi: 10.1007/s11430-013-4773-4, 2014.

925  
926 Wang, Z. F., Li, J., Wang, Z., Yang, W. Y., Tang, X., Ge, B. Z., Yan, P. Z., Zhu, L. L.,  
927 Chen, X. S., Chen, H. S., Wang, W., Li, J. J., Liu, B., Wang, X. Y., Wand, W., Zhao, Y.  
928 L., Lu, N., and Su, D. B.: Modeling study of regional severe hazes over mid-eastern  
929 China in January 2013 and its implications on pollution prevention and control, *Sci.*  
930 *China-Earth Sci.*, 57, 3–13, doi: 10.1007/s11430-013-4793-0, 2014.

931  
932 Wei, C.: Modeling the effects of heterogeneous reactions on atmospheric chemistry  
933 and aerosol properties, PhD Diss., University of Iowa, <http://ir.uiowa.edu/etd/903> (last  
934 access: June 2014), 2010.

935  
936 Whitten, G. Z., Heo, G., Kimura, Y., McDonald-Buller, E., Allen, D. T., Carter, W. P.  
937 L., and Yarwood, G.: A new condensed toluene mechanism for Carbon Bond: CB05-  
938 TU, *Atmos. Environ.*, 44, 5346–5355, doi: 10.1016/j.atmosenv.2009.12.029, 2010.

939  
940 Wu, L. Y., Tong, S. R., Wang, W. G., and Ge, M. F.: Effects of temperature on the  
941 heterogeneous oxidation of sulfur dioxide by ozone on calcium carbonate, *Atmos.*  
942 *Chem. Phys.*, 11, 6593–6605, doi: 10.5194/acp-11-6593-2011, 2011.

943  
944 Xiu, A., and Pleim, J. E.: Development of a Land Surface Model. Part I: Application  
945 in a Mesoscale Meteorological Model, *J. Appl. Meteorol.*, 40, 192–209, doi:  
946 10.1175/1520-0450(2001)040<0192:doalsm>2.0.co;2, 2001.

947  
948 Yang, F., Tan, J., Zhao, Q., Du, Z., He, K., Ma, Y., Duan, F., and Chen, G.:  
949 Characteristics of PM<sub>2.5</sub> speciation in representative megacities and across China,  
950 *Atmos. Chem. Phys.*, 11, 5207–5219, doi: 10.5194/acp-11-5207-2011, 2011.

951  
952 Yang, K., Dickerson, R. R., Carn, S. A., Ge, C., and Wang, J.: First observations of  
953 SO<sub>2</sub> from the satellite Suomi NPP OMPS: Widespread air pollution events over  
954 China, *Geophys. Res. Lett.*, 40, 4957–4962, doi: 10.1002/grl.50952, 2013.

955  
956 Zhang, J. K., Sun, Y., Liu, Z. R., Ji, D. S., Hu, B., Liu, Q., and Wang, Y. S.:  
957 Characterization of submicron aerosols during a month of serious pollution in Beijing,  
958 2013, *Atmos. Chem. Phys.*, 14, 2887–2903, doi: 10.5194/acp-14-2887-2014, 2014.  
959  
960 Zhang, Q., Streets, D. G., He, K., Wang, Y., Richter, A., Burrows, J. P., Uno, I., Jang,  
961 C. J., Chen, D., Yao, Z., and Lei, Y.: NO<sub>x</sub> emission trends for China, 1995–2004: The  
962 view from the ground and the view from space, *J. Geophys. Res.-Atmos.*, 112,  
963 D22306, doi: 10.1029/2007jd008684, 2007.  
964  
965 Zhang, Q., Streets, D. G., Carmichael, G. R., He, K. B., Huo, H., Kannari, A.,  
966 Klimont, Z., Park, I. S., Reddy, S., Fu, J. S., Chen, D., Duan, L., Lei, Y., Wang, L. T.,  
967 and Yao, Z. L.: Asian emissions in 2006 for the NASA INTEX-B mission, *Atmos.*  
968 *Chem. Phys.*, 9, 5131–5153, doi: 10.5194/acp-9-5131-2009, 2009.  
969  
970 Zhang, R. H., Li, Q., and Zhang, R. N.: Meteorological conditions for the persistent  
971 severe fog and haze event over eastern China in January 2013, *Sci. China-Earth Sci.*,  
972 57, 26–35, doi: 10.1007/s11430-013-4774-3, 2014.  
973  
974 Zhang, Y., and Carmichael, G. R.: The Role of Mineral Aerosol in Tropospheric  
975 Chemistry in East Asia—A Model Study, *J. Appl. Meteorol.*, 38, 353–366, doi:  
976 10.1175/1520-0450(1999)038<0353:tromai>2.0.co;2, 1999.  
977  
978 Zhang, Y., Sunwoo, Y., Kotamarthi, V., and Carmichael, G. R.: Photochemical  
979 Oxidant Processes in the Presence of Dust: An Evaluation of the Impact of Dust on  
980 Particulate Nitrate and Ozone Formation, *J. Appl. Meteorol.*, 33, 813–824, doi:  
981 10.1175/1520-0450(1994)033<0813:popitp>2.0.co;2, 1994.  
982  
983 Zhang, Y., Liu, P., Pun, B., and Seigneur, C.: A comprehensive performance  
984 evaluation of MM5-CMAQ for the Summer 1999 Southern Oxidants Study episode—  
985 Part I: Evaluation protocols, databases, and meteorological predictions, *Atmos.*  
986 *Environ.*, 40, 4825–4838, doi: 10.1016/j.atmosenv.2005.12.043, 2006.  
987  
988 Zhang, Y., Cheng, S.-H., Chen, Y.-S., and Wang, W.-X.: Application of MM5 in  
989 China: Model evaluation, seasonal variations, and sensitivity to horizontal grid  
990 resolutions, *Atmos. Environ.*, 45, 3454–3465, doi: 10.1016/j.atmosenv.2011.03.019,  
991 2011.  
992  
993 Zhang, Y., Chen, Y., Sarwar, G., and Schere, K.: Impact of gas-phase mechanisms on  
994 Weather Research Forecasting Model with Chemistry (WRF/Chem) predictions:  
995 Mechanism implementation and comparative evaluation, *J. Geophys. Res.-Atmos.*,  
996 117, D01301, doi: 10.1029/2011jd015775, 2012.  
997  
998 Zhao, B., Wang, S., Wang, J., Fu, J. S., Liu, T., Xu, J., Fu, X., and Hao, J.: Impact of

999 national NO<sub>x</sub> and SO<sub>2</sub> control policies on particulate matter pollution in China,  
1000 Atmos. Environ., 77, 453–463, doi: 10.1016/j.atmosenv.2013.05.012, 2013.  
1001  
1002 Zhao, P., Zhang, X., Xu, X., and Zhao, X.: Long-term visibility trends and  
1003 characteristics in the region of Beijing, Tianjin, and Hebei, China, Atmos. Res., 101,  
1004 711–718, doi: 10.1016/j.atmosres.2011.04.019, 2011.  
1005 Zhao, X. J., Zhao, P. S., Xu, J., Meng, W., Pu, W. W., Dong, F., He, D., and Shi, Q. F.:  
1006 Analysis of a winter regional haze event and its formation mechanism in the North  
1007 China Plain, Atmos. Chem. Phys., 13, 5685–5696, doi: 10.5194/acp-13-5685-2013,  
1008 2013.  
1009  
1010 Zhao, Y., Duan, L., Xing, J., Larssen, T., Nielsen, C. P., and Hao, J.: Soil Acidification  
1011 in China: Is Controlling SO<sub>2</sub> Emissions Enough?, Environ. Sci. Technol., 43, 8021–  
1012 8026, doi: 10.1021/es901430n, 2009.  
1013  
1014 Zheng, B., Huo, H., Zhang, Q., Yao, Z. L., Wang, X. T., Yang, X. F., Liu, H., and He,  
1015 K. B.: High-resolution mapping of vehicle emissions in China in 2008, Atmos. Chem.  
1016 Phys., 14, 9787–9805, doi:10.5194/acp-14-9787-2014, 2014.  
1017  
1018 Zheng, G. J., Duan, F. K., Ma, Y. L., Cheng, Y., Zheng, B., Zhang, Q., Huang, T.,  
1019 Kimoto, T., Chang, D., Su, H., Pöschl, U., Cheng, Y. F., and He, K. B.: Exploring the  
1020 severe winter haze in Beijing, Atmos. Chem. Phys. Discuss., 14, 17907–17942,  
1021 doi:10.5194/acpd-14-17907-2014, 2014.  
1022

1023  
1024

Table 1. Main reactions contributing to sulfate and nitrate production in original CMAQ and heterogeneous reactions newly added in revised CMAQ

Type	Reaction #.	Reaction	Contributions to PM <sub>2.5</sub>
<b>original CMAQ</b>			
Gas-phase chemistry (All species in gas phase)	R1	$\text{SO}_2 + \text{OH} + \text{H}_2\text{O} + \text{O}_2 \rightarrow \text{H}_2\text{SO}_4 + \text{HO}_2$	Sulfate
	R2	$\text{NO}_2 + \text{OH} \rightarrow \text{HNO}_3$	Nitrate
	R3	$\text{N}_2\text{O}_5 + \text{H}_2\text{O} \rightarrow 2\text{HNO}_3$	Nitrate
	R4	$\text{NO}_3 + \text{HO}_2 \rightarrow \text{HNO}_3 + \text{O}_2$	Nitrate
	R5	$\text{NTR}^a + \text{OH} \rightarrow \text{HNO}_3$	Nitrate
	R6	$\text{NO}_3 + \text{VOCs}^b \rightarrow \text{HNO}_3$	Nitrate
Aqueous-phase kinetic chemistry (All species in aqueous phase)	R7	$\text{HSO}_3^- + \text{H}_2\text{O}_2 \rightarrow \text{SO}_4^{2-} + \text{H}^+ + \text{H}_2\text{O}$	Sulfate
	R8	$\text{HSO}_3^- + \text{MHP}^c \rightarrow \text{SO}_4^{2-} + \text{H}^+$	Sulfate
	R9	$\text{HSO}_3^- + \text{PAA}^d \rightarrow \text{SO}_4^{2-} + \text{H}^+$	Sulfate
	R10	$\text{SO}_2 + \text{O}_3 + \text{H}_2\text{O} \rightarrow \text{SO}_4^{2-} + 2\text{H}^+ + \text{O}_2$	Sulfate
	R11	$\text{HSO}_3^- + \text{O}_3 \rightarrow \text{SO}_4^{2-} + \text{H}^+ + \text{O}_2$	Sulfate
	R12	$\text{SO}_3^{2-} + \text{O}_3 \rightarrow \text{SO}_4^{2-} + \text{O}_2$	Sulfate
	R13	$\text{SO}_2 + \text{H}_2\text{O} + 0.5\text{O}_2 + \text{Fe(III)/Mn(II)} \rightarrow \text{SO}_4^{2-} + 2\text{H}^+$	Sulfate
Heterogeneous chemistry	R14	$\text{N}_2\text{O}_5 (\text{g}) + \text{H}_2\text{O} (\text{aq}) \rightarrow 2\text{HNO}_3 (\text{aq})$	Nitrate
	R15	$2\text{NO}_2 (\text{g}) + \text{H}_2\text{O} (\text{aq}) \rightarrow \text{HONO} (\text{aq}) + \text{HNO}_3 (\text{aq})$	Nitrate
<b>revised CMAQ</b>			
Newly added heterogeneous chemistry	R16	$\text{H}_2\text{O}_2 (\text{g}) + \text{Aerosol} \rightarrow \text{Products}$	Affect R7
	R17	$\text{HNO}_3 (\text{g}) + \text{Aerosol} \rightarrow 0.5\text{NO}_3^- + 0.5\text{NO}_x (\text{g})$	Renoxification
	R18	$\text{HO}_2 (\text{g}) + \text{Fe(II)} \rightarrow \text{Fe(III)} + \text{H}_2\text{O}_2$	Affect R4 and R7
	R19	$\text{N}_2\text{O}_5 (\text{g}) + \text{Aerosol} \rightarrow 2\text{NO}_3^-$	Nitrate
	R20	$\text{NO}_2 (\text{g}) + \text{Aerosol} \rightarrow \text{NO}_3^-$	Nitrate
	R21	$\text{NO}_3 (\text{g}) + \text{Aerosol} \rightarrow \text{NO}_3^-$	Nitrate
	R22	$\text{O}_3 (\text{g}) + \text{Aerosol} \rightarrow \text{Products}$	Affect R10–R12
	R23	$\text{OH} (\text{g}) + \text{Aerosol} \rightarrow \text{Products}$	Affect R1–R2, R5
	R24	$\text{SO}_2 (\text{g}) + \text{Aerosol} \rightarrow \text{SO}_4^{2-}$	Sulfate

1025  
1026  
1027  
1028  
1029  
1030

<sup>a</sup> NTR: organic nitrate.

<sup>b</sup> VOCs include: formaldehyde, acetaldehyde, propionaldehyde and higher aldehydes, cresol and higher molecular weight phenols, nitro cresol, aromatic ring open products, and isoprene oxidation products.

<sup>c</sup> MHP: methylhydroperoxide.

<sup>d</sup> PAA: peroxyacetic acid.

Table 2. Domain, configurations, and major physical options used in WRF v3.5.1

Simulation period	Dec 2012 and Jan 2013
Domain	East Asia (Columns:178, Rows: 133) with 3 extra grids in each boundary of Domain 1 (Columns:172, Rows: 127)
Horizontal resolution	36 km
Vertical resolution	23 sigma levels from surface to tropopause (about 100 mb)
Meteorological IC and BC	Reanalysis data from the National Centers for Environmental Prediction Final Analysis (NCEP-FNL)
Shortwave radiation	New Goddard scheme (Chou et al., 1998)
Longwave radiation	The rapid radiative transfer model (RRTM) (Mlawer et al., 1997)
Land surface model	The USGS 24-category land use data
Surface layer	Pleim-Xiu land surface scheme (Xiu and Pleim, 2001)
Planetary boundary layer model	ACM2 PBL scheme (Pleim, 2007)
Cumulus parameterization	Kain-Fritsch cumulus scheme (Kain, 2004)
Cloud microphysics	WSM6 (Hong and Lim, 2006)
Analysis nudging	Temperature and water vapor mixing (above PBL); wind (in and above PBL)
Observational nudging	Temperature, water vapor mixing and wind (in and above PBL)
Soil nudging	Include soil moisture and temperature
FDDA data	NCEP Automated Data Processing (ADP) surface (ds461.0) and upper (ds351.0) air data



Table 3. Domain, configurations, and options used in CMAQ v5.0.1

Simulation period	25 Dec 2012 to 31 Jan 2013
Domain	Domain 1 (Columns:172, Rows: 127)
Horizontal resolution	36 km
Vertical resolution	14 sigma levels from surface to tropopause. The values of sigma levels are: 1.000, 0.995, 0.988, 0.980, 0.970, 0.956, 0.938, 0.893, 0.839, 0.777, 0.702, 0.582, 0.400, 0.200, and 0.000.
IC and BC	GEOS-Chem 2° × 2.5° global simulation
Gas-phase mechanism	CB05 gas-phase mechanism with active chlorine chemistry and updated toluene mechanism of Whitten et al. (2010)
Aqueous-phase mechanism	The updated mechanism of the RADM model (Walcek and Taylor, 1986; Chang et al., 1987)
Aerosol module	AERO6
Photolytic rate	Calculate photolytic rates in-line using simulated aerosols and ozone concentrations
Cloud module	ACM cloud processor that uses the ACM methodology to compute convective mixing for AERO6
Windblown dust	The physical-based dust emission algorithm FENGSHA ( <a href="http://www.airqualitymodeling.org/cmaqwiki/index.php?title=CMAQv5.0_Windblown_Dust">http://www.airqualitymodeling.org/cmaqwiki/index.php?title=CMAQv5.0_Windblown_Dust</a> )
Lightning NO <sub>x</sub>	Not included, due to extremely low flash rates over the East Asia in winter (Schumann and Huntrieser, 2007)

Table 4. Simulation design

Run Index	Emission	Meteorology	Model configuration	Purpose
Original CMAQ	Jan. 2013	Jan. 2013	original CMAQ	Examine the capability and limitation of the original model to study severe haze pollution
Revised CMAQ	Jan. 2013	Jan. 2013	revised CMAQ with heterogeneous chemistry	Evaluate the role of heterogeneous chemistry in haze pollution
Revised CMAQ with 2013Emis&2012Met	Jan. 2013	Jan. 2012	revised CMAQ with heterogeneous chemistry	Evaluate the impact of meteorological anomaly of 2013 on sulfate and nitrate production

1035

Table 5. Observational data for model evaluation.

Dataset	Data	Variable <sup>d</sup>	Frequency	Site number	Time period	Sources
NCDC <sup>a</sup>	Meteorology	T2, RH2, WS10, WD10, Precip	Every 1 or 3 h	~1000	1–31 Jan 2013	<a href="ftp://ftp.ncdc.noaa.gov/pub/data/noaa/">ftp://ftp.ncdc.noaa.gov/pub/data/noaa/</a>
CNEMC <sup>b</sup>	Gaseous and particulate species	SO <sub>2</sub> , NO <sub>2</sub> , CO, PM <sub>2.5</sub> , and PM <sub>10</sub>	Hourly	496	1–31 Jan 2013	<a href="http://113.108.142.147:20035/emcpublish/">http://113.108.142.147:20035/emcpublish/</a>
THU <sup>c</sup>	Particulate species	PM <sub>2.5</sub> , SO <sub>4</sub> <sup>2-</sup> , NO <sub>3</sub> <sup>-</sup> , NH <sub>4</sub> <sup>+</sup> , EC, OC	Hourly	1	1–31 Jan 2013	G. J. Zheng et al. (2014)

1036 <sup>a</sup> NCDC: Meteorological data obtained from the National Climate Data Center.1037 <sup>b</sup> CNEMC: Gaseous and particulate concentrations obtained from the China National Environmental  
1038 Monitoring Center.1039 <sup>c</sup> THU: Particulate species concentration measured at Tsinghua University.1040 <sup>d</sup> T2: Temperature at 2 m; RH2: Relative humidity at 2 m; WS10: wind speed at 10 m; WD10: wind  
1041 direction at 10 m; Precip: daily Precipitation.

1042

1043

Table 6. Performance statistics of WRF simulation

	T2 <sup>a</sup>	RH2 <sup>a</sup>	WS10 <sup>a</sup>	WD10 <sup>a</sup>	Precip <sup>a</sup>
Data pairs <sup>b</sup>	385753	385103	385165	336507	488
MeanObs <sup>b</sup>	-0.2	67.5	2.7	227.1	1.8
MeanSim <sup>b</sup>	-1.1	74.1	3.0	205.6	2.9
R <sup>b</sup>	1.0	0.7	0.6	0.3	0.4
MB <sup>b</sup>	-0.8	6.7	0.3	-21.6	1.1
RMSE <sup>b</sup>	3.5	14.9	2.1	177.2	7.9
NMB(%) <sup>b</sup>	-389.5	9.9	9.5	-9.5	58.8
NME(%) <sup>b</sup>	1211.3	17	57.9	41.9	145

1044 <sup>a</sup> Definitions of these variables can be found in the footnotes of Table 5. The units of T2, RH2, WS10,  
 1045 WD10, and Precip are °C, %, m s<sup>-1</sup>, degree, and mm day<sup>-1</sup>, respectively. The T2, RH2, WS10 and  
 1046 WD10 are evaluated using hourly data and the Precip is evaluated using daily data.

1047 <sup>b</sup> Data pairs: the number of observed and simulated data pairs; MeanObs: mean observational data;  
 1048 MeanSim: mean simulation results; R: correlation coefficient; MB: mean bias; RMSE: root mean  
 1049 square error; NMB: normalized mean bias; NME: normalized mean error.

1050 Table 7. Performance statistics of the original and revised CMAQ model at the THU  
 1051 site

		PM <sub>2.5</sub> <sup>a</sup>	SO <sub>4</sub> <sup>2-</sup>	NO <sub>3</sub> <sup>-</sup>	NH <sub>4</sub> <sup>+</sup>	EC	OC
Obs		186.0	32.8	30.7	20.8	4.2	47.3
Original CMAQ	MeanSim	145.2	15.0	18.4	8.7	12.3	35.3
	R	0.8	0.6	0.8	0.7	0.6	0.8
	MB	-40.8	-17.8	-12.3	-12.1	8.2	-12.0
	RMSE	102.3	30.5	19.6	18.5	9.0	19.9
	NMB(%)	-21.9	-54.2	-40.0	-58.1	196.2	-25.3
	NME(%)	33.8	57.4	42.0	59.0	196.2	29.2
Revised CMAQ	MeanSim	186.8	34.8	32.4	19.9	11.8	34.2
	R	0.8	0.7	0.8	0.8	0.6	0.7
	MB	0.8	2.1	1.8	-0.8	7.6	-13.1
	RMSE	83.3	21.2	14.6	11.6	8.4	21.2
	NMB(%)	0.4	6.3	5.7	-4.1	183.0	-27.8
	NME(%)	33.1	46.8	35.3	39.4	183.8	31.7

1052 <sup>a</sup> The units of PM<sub>2.5</sub>, SO<sub>4</sub><sup>2-</sup>, NO<sub>3</sub><sup>-</sup>, NH<sub>4</sub><sup>+</sup>, OC, and EC are all µg m<sup>-3</sup>.

1053

1054 Table 8. Domain-wide performance statistics of the original and revised CMAQ

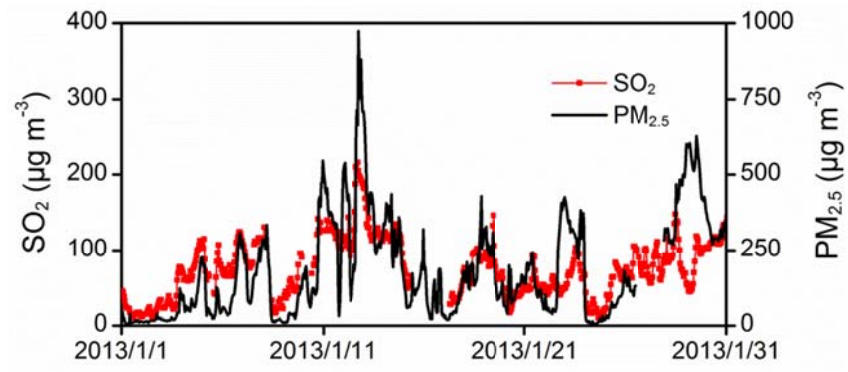
	CO <sup>a</sup>		NO <sub>2</sub> <sup>a</sup>		SO <sub>2</sub> <sup>a</sup>		PM <sub>2.5</sub> <sup>a</sup>		PM <sub>10</sub> <sup>a</sup>	
	Original	Revised	Original	Revised	Original	Revised	Original	Revised	Original	Revised
Data pairs	9338	9338	9366	9366	9384	9384	9335	9335	9143	9143
MeanObs	2.3	2.3	66.9	66.9	86.7	86.7	142.9	142.9	202.2	202.2
MeanSim	1.8	1.8	75.8	74.3	131.0	120.0	154.4	180.2	179.5	203.3
R	0.5	0.5	0.5	0.4	0.4	0.4	0.6	0.6	0.6	0.6
MB	-0.5	-0.5	9.0	7.5	44.4	33.4	11.5	37.3	-22.7	1.2
RMSE	1.5	1.5	35.3	34.1	119.1	110.5	86.9	111.0	116.1	122.5
NMB(%)	-20.6	-20.5	13.4	11.2	51.2	38.5	8.1	26.1	-11.2	0.6
NME(%)	43.3	43.3	41.9	39.4	91.6	84.6	41.3	54.3	38.1	42.4

1055 <sup>a</sup> The units of CO, NO<sub>2</sub>, SO<sub>2</sub>, PM<sub>2.5</sub>, and PM<sub>10</sub> are mg m<sup>-3</sup>, µg m<sup>-3</sup>, µg m<sup>-3</sup>, µg m<sup>-3</sup>, and µg m<sup>-3</sup>,  
 1056 respectively.

1057

1058

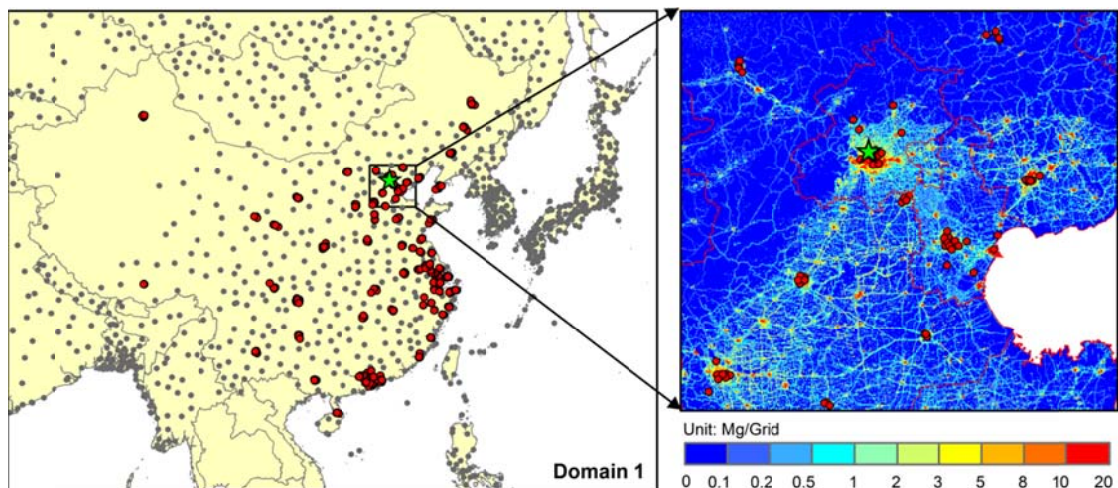
1059



1061

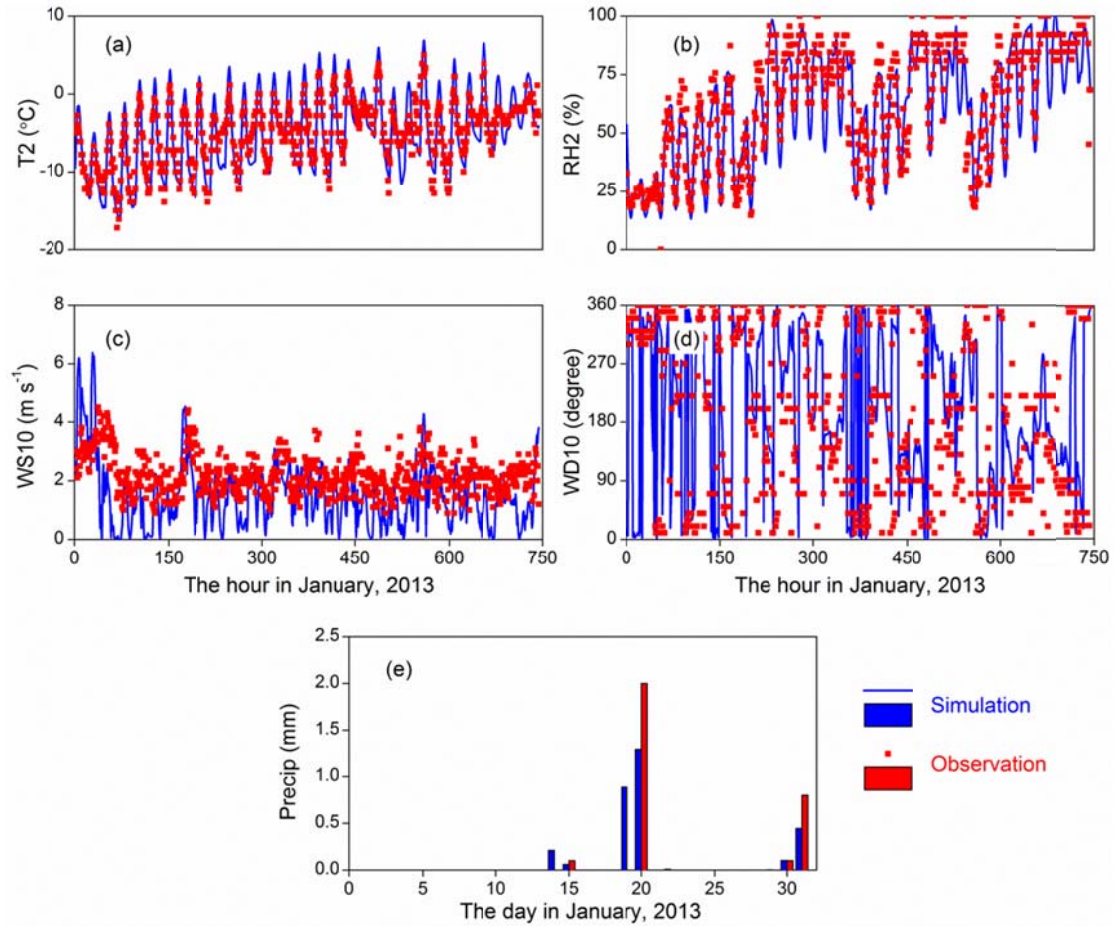
1062

Figure 1. Observed concentrations of SO<sub>2</sub> and PM<sub>2.5</sub> during January 2013 in Beijing.



1063

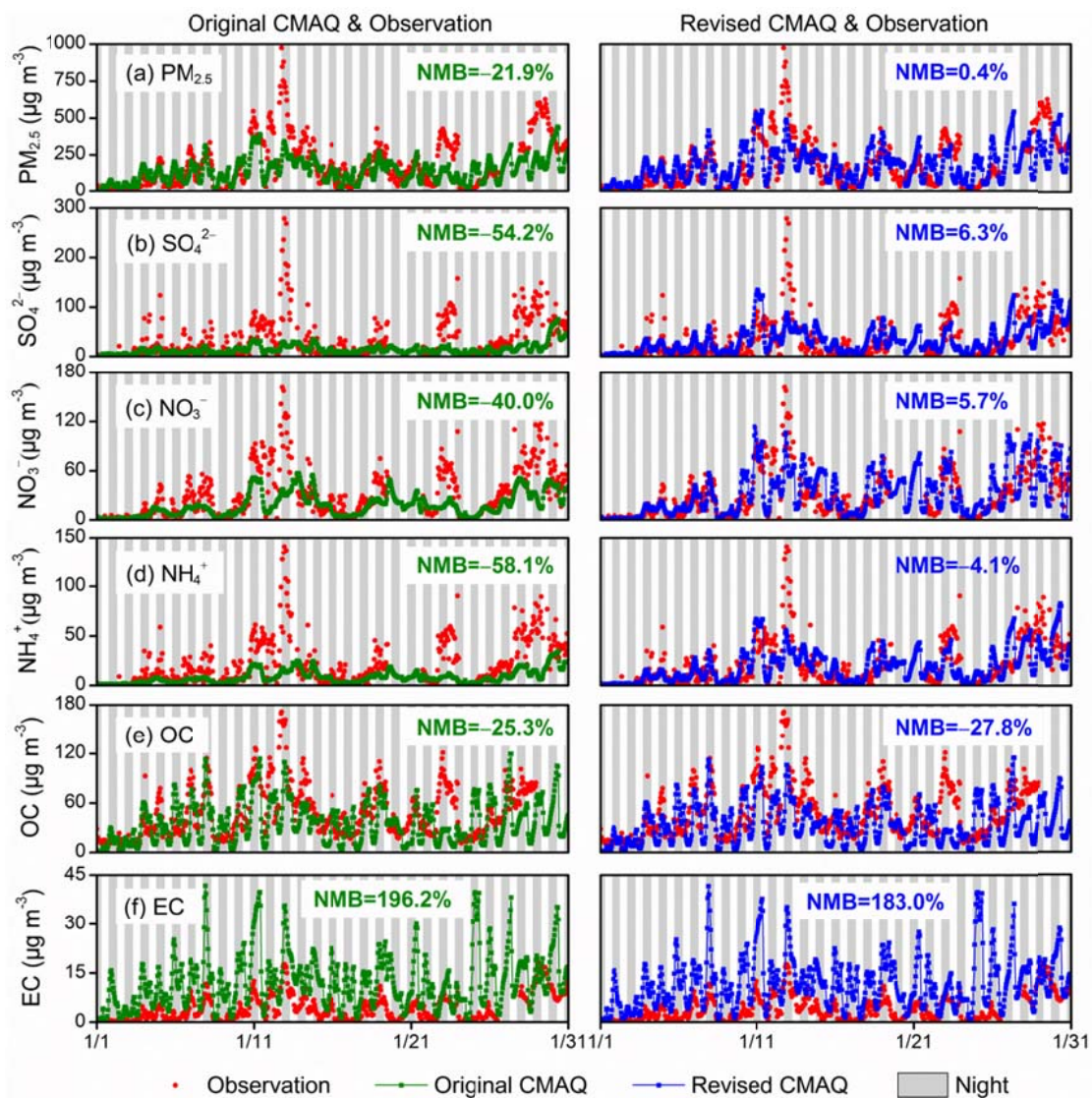
1068 **Figure 2.** Simulation domain (Domain 1) and the monitoring stations. Gray circles are  
 1069 meteorological stations included in the NCDC dataset and red circles are monitoring  
 1070 stations included in the CNEMC dataset. Green star is the monitoring station at THU.  
 1071 Background in the enlarged map is NO<sub>x</sub> emission inventory of January 2013 at a  
 1072 horizontal resolution of 1 km.



1069

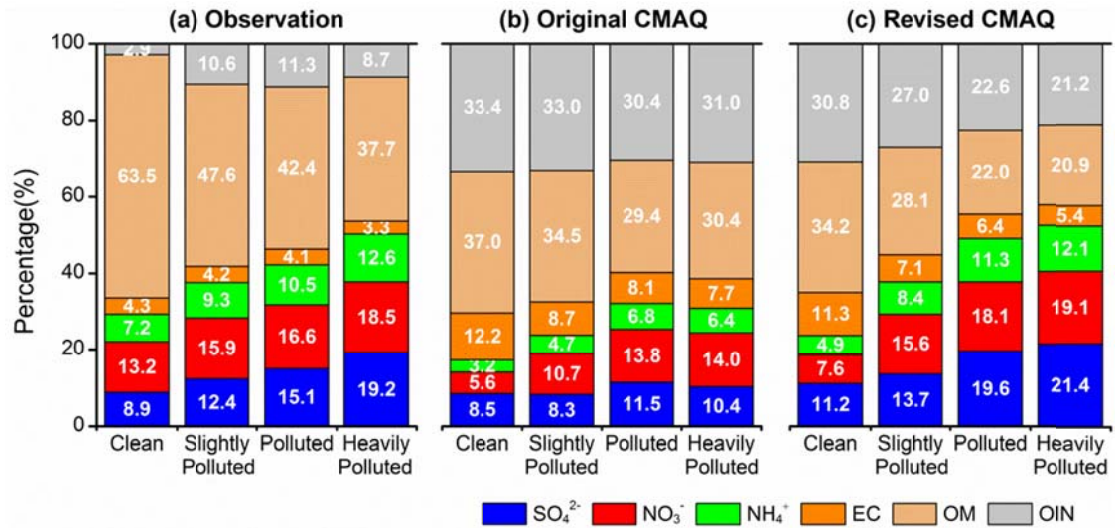
1071 **Figure 3.** Observed and simulated meteorological variables at THU site: (a) hourly  
 1072 T2; (b) hourly RH2; (c) hourly WS10; (d) hourly WD10; (e) daily Precip.





1072  
 1075  
 1076  
 1077

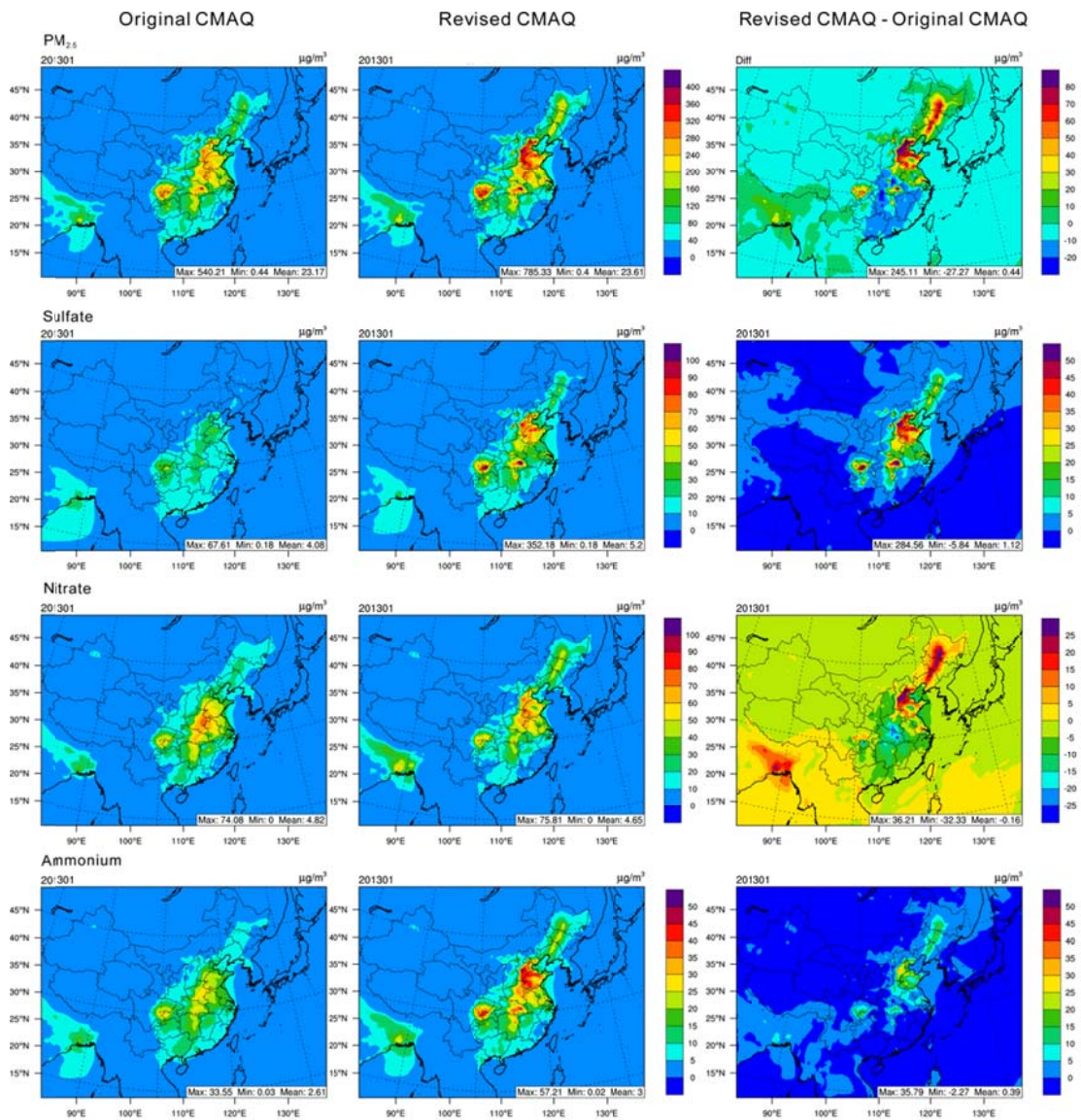
**Figure 4.** Observed and simulated hourly aerosol compositions from the original and revised CMAQ at the THU site: (a)  $PM_{2.5}$ ; (b)  $SO_4^{2-}$ ; (c)  $NO_3^-$ ; (d)  $NH_4^+$ ; (e) OC; (f) EC.



1076

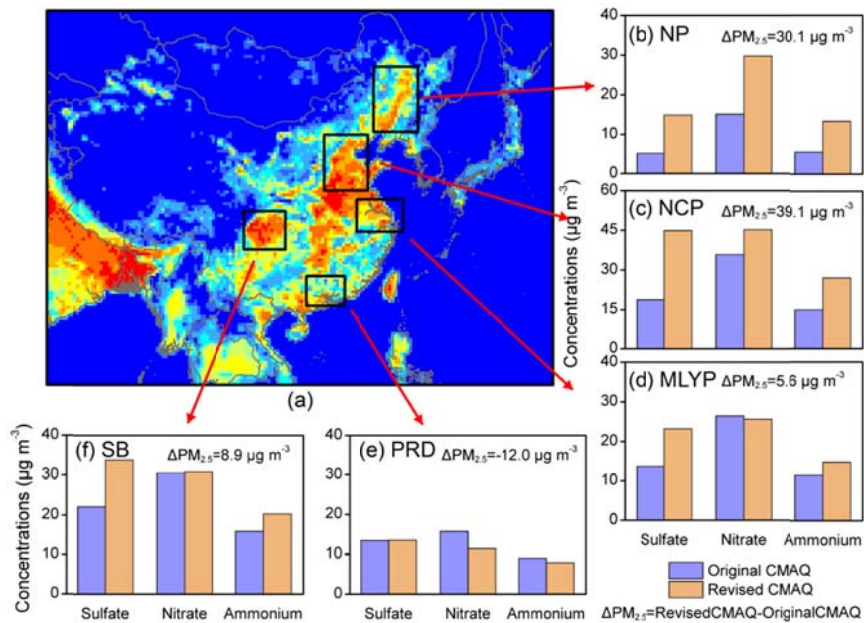
1084 **Figure 5.** Percentile compositions of major components in PM<sub>2.5</sub> derived from (a)  
 1085 Observation; (b) Original CMAQ; (c) Revised CMAQ with enhanced heterogeneous  
 1086 chemistry. The pollution is classified into four types: clean (PM<sub>2.5</sub> ≤ 35 μg m<sup>-3</sup>),  
 1087 slightly polluted (35 < PM<sub>2.5</sub> ≤ 115 μg m<sup>-3</sup>), polluted (115 < PM<sub>2.5</sub> ≤ 350 μg m<sup>-3</sup>), and  
 1088 heavily polluted (PM<sub>2.5</sub> > 350 μg m<sup>-3</sup>), based on the China's Air Quality Index (AQI)  
 1089 level definition.

1090 (<http://kjs.mep.gov.cn/hjbhbz/bzwb/dqhjbh/jcgfffbz/201203/W020120410332725219>  
 1091 541.pdf)



1085  
 1089  
 1090  
 1091  
 1092

**Figure 6.** Spatial distributions of monthly (January 2013) mean concentrations of PM<sub>2.5</sub>, sulfate, nitrate, and ammonium simulated by the Original CMAQ (left), Revised CMAQ (middle), and the differences between the Revised and Original CMAQ (right).



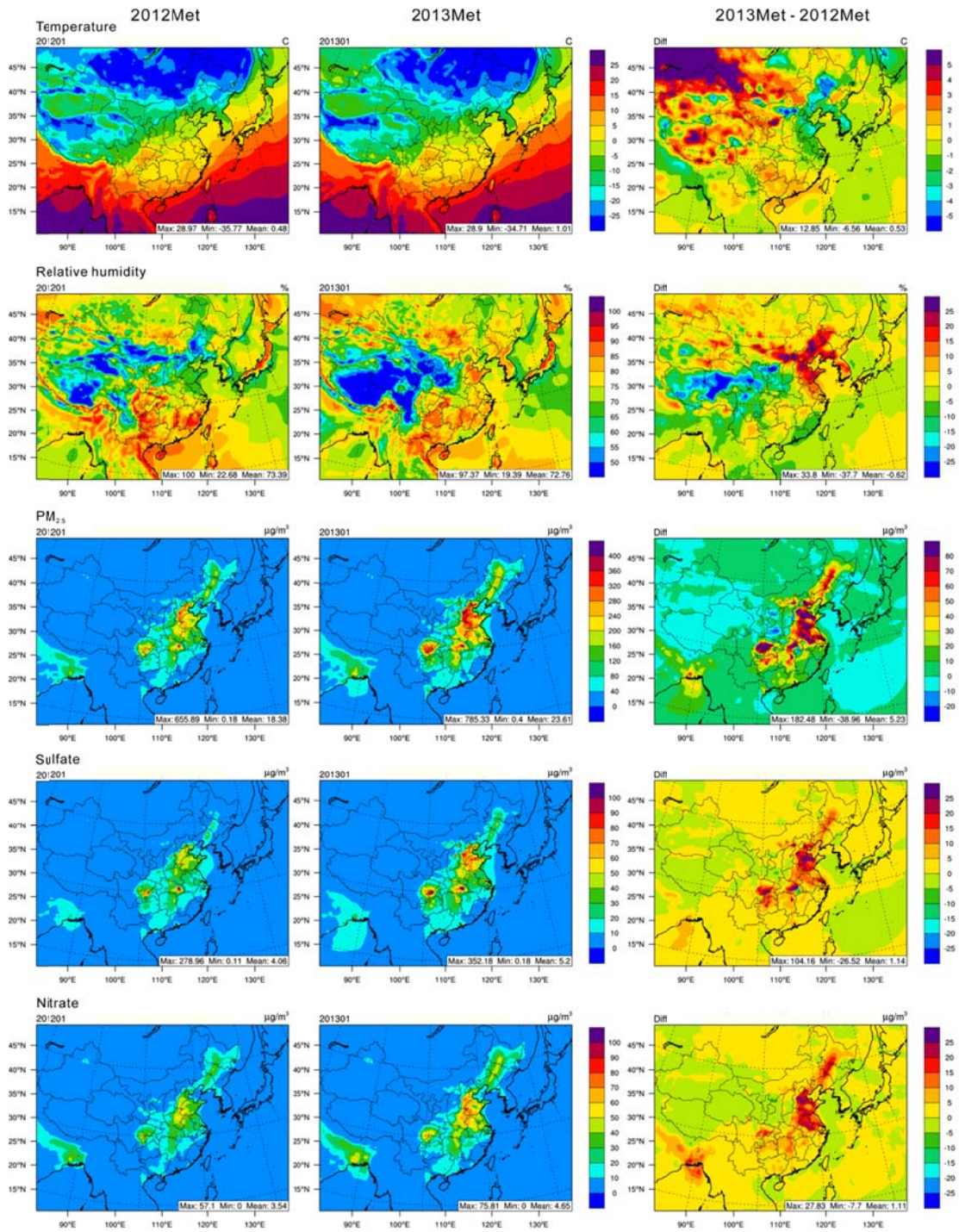
1090

1093

1094

1095

Figure 7. Comparison of predicted SNA from Original and Revised CMAQ for (b) NP, (c) NCP, (d) MLYP, (e) PRD and (f) SB. The figure (a) is the emission map of  $\text{NH}_3$  in January 2013 at a horizontal resolution of 36 km (source: MEIC model).



1094

1098 **Figure 8.** Spatial distributions of the monthly (January 2013) mean temperature, RH,  
 1099 and concentrations of  $PM_{2.5}$ , sulfate, and nitrate simulated by the revised CMAQ  
 1100 model with meteorological fields of 2012 (left) and 2013 (middle), and the differences  
 1101 between these two simulations (right).  
 1099